The Current and Future Impact of CFD:

Advances in the High-Order Spectral Difference Method

Antony Jameson
Thomas V. Jones Professor of Engineering
Aeronautics and Astronautics Department
Stanford University

Florida State University Lecture Series, February 15-20, 2010

OVERVIEW

Emergence of CFD

Emergence of CFD 1965–2005

- In 1960 the underlying principles of fluid dynamics and the formulation of the governing equations (potential flow, Euler, RANS) were well established.

- The new element was the emergence of powerful enough computers to make numerical solution possible –to carry this out required new algorithms.

- The emergence of CFD in the 1965–2005 period depended on a conbination of advances in computer power and algorithms.

Multidisciplinary Nature of CFD

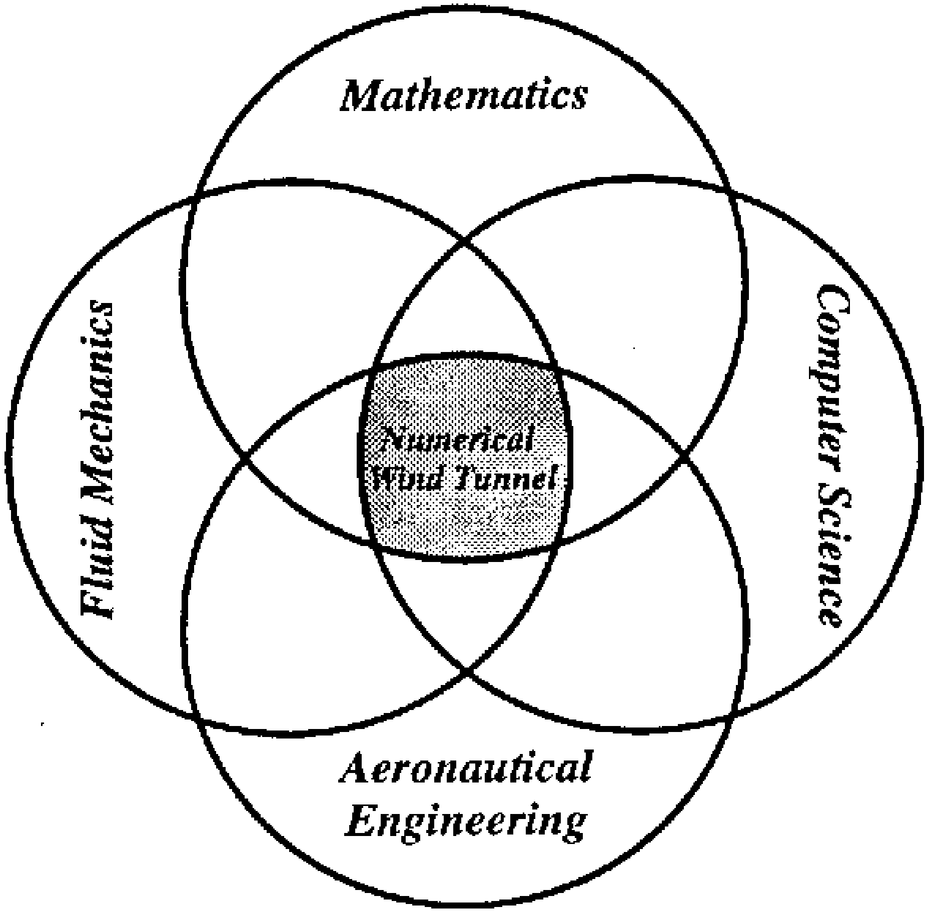

Hierarchy of Equations

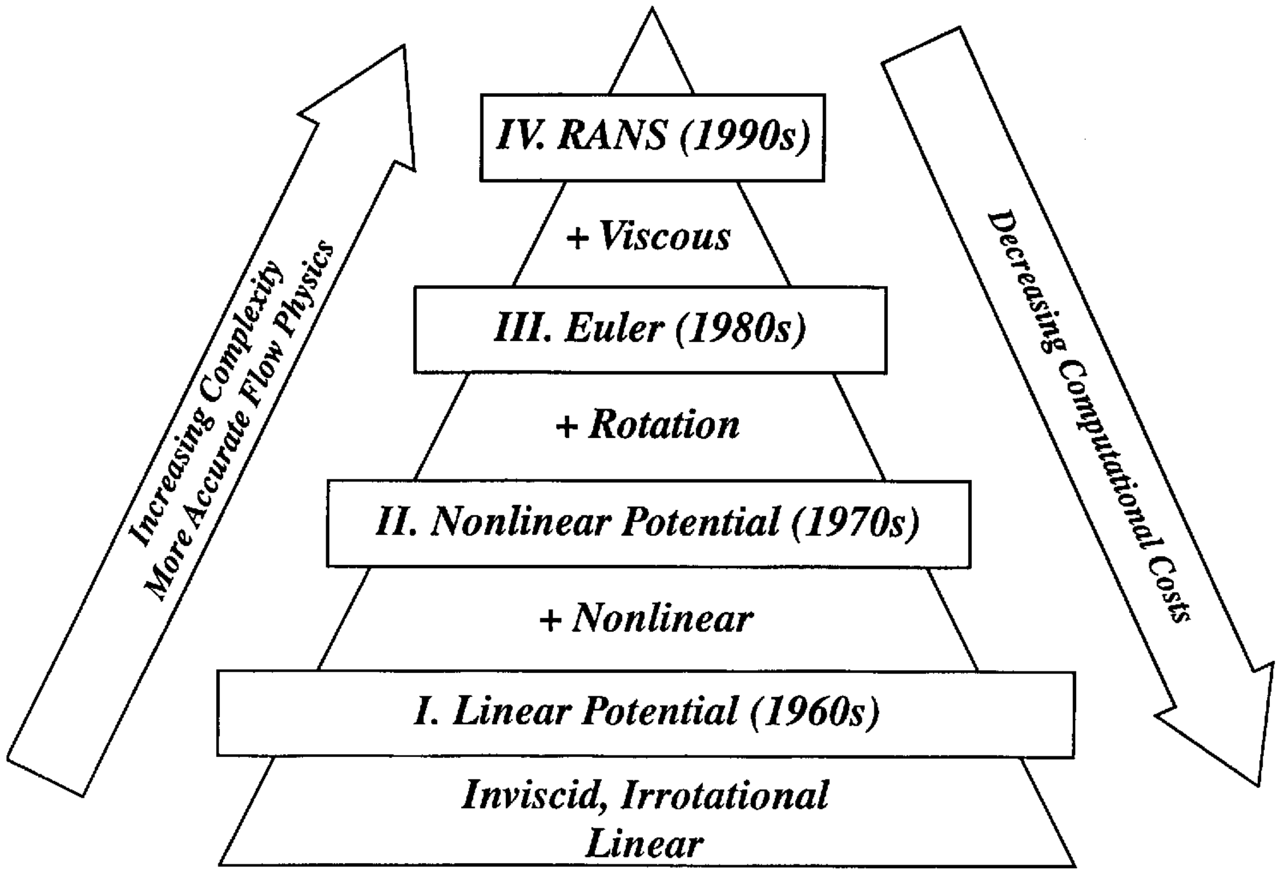

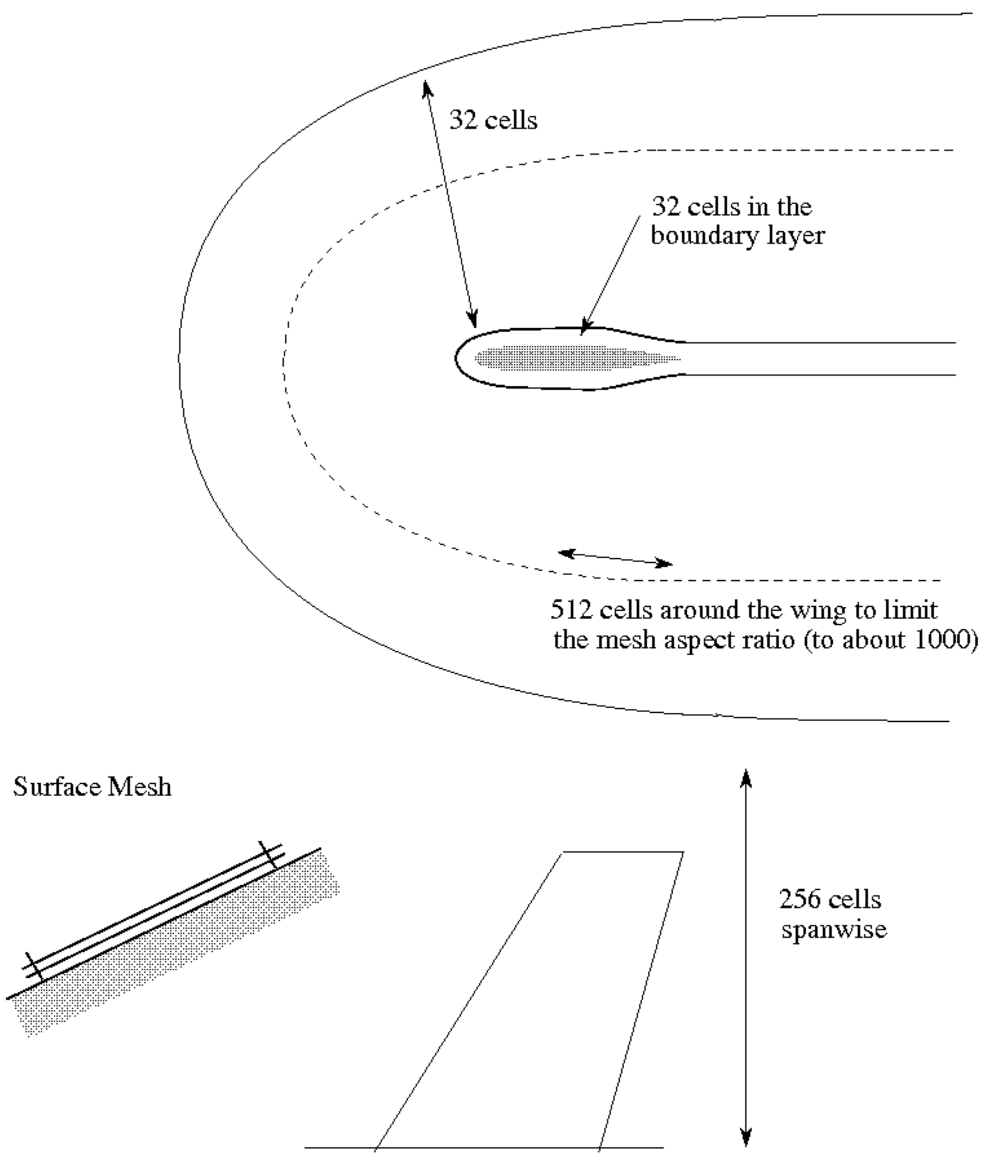

Total: 512 x 64 x 256 = 8 388 608 cells

Advances in Computers

1970	CFD 6600	1	Megaflops	10^6
1980	Cray 1			
	vector computer	100	Megaflops	10^8
1994	IBM SP2			
	parallel computer	10	Gigaflops	10^{10}
2007	Linux clusters	100	Teraflops	10^{14}
2007	(affordable) BoxCluster in my house			
	Four 3 GHz dual core CPUs			
	(24 Gigaflops peak)	5	Gigaflops	5×10^9
	$10,000			
2009	HP Pavilion quadcore Notebook			
	$1,099	1	Gigaflops	1×10^9

Early Use of Flo22 At McDonnell Douglas

Wing Configuration Matrix

AERODYNAMIC DEVELOPMENT

WING CONFIGURATION MATRIX EVALUATED

WITH THE 3-D DOUGLAS-JAMESON TRANSONIC PROGRAM

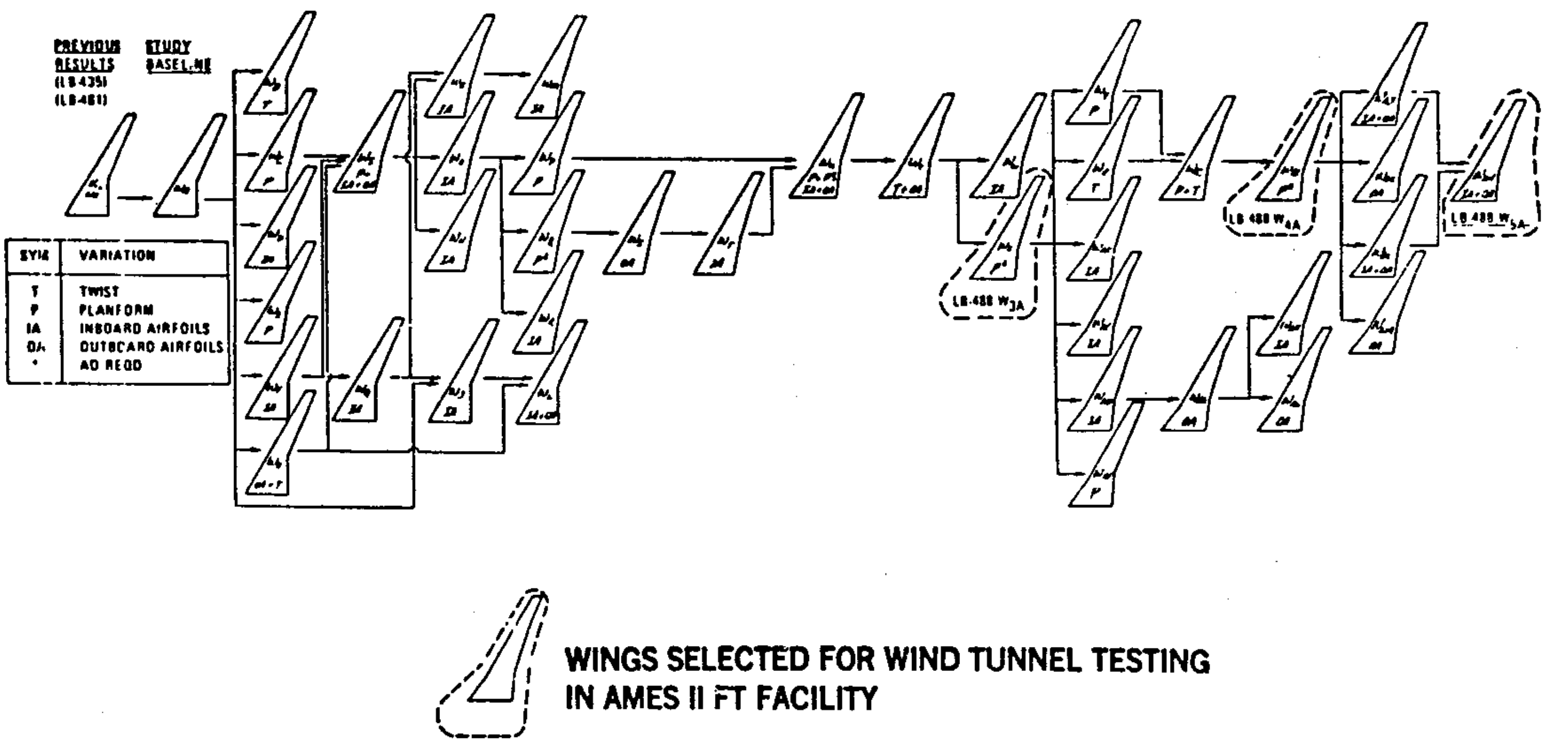

8-DC10-10200A

Flo57
Euler solution on structured mesh using JST

Precursor to

Lockheed TEAM

NASA TLNS3D

BAE EJ65

Dornier Ikarus

Northrop YF-23

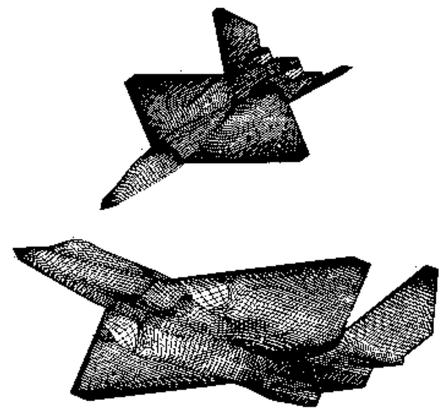

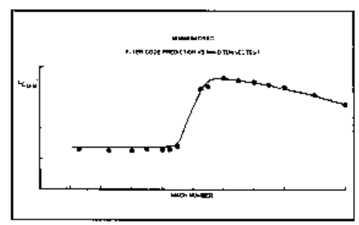

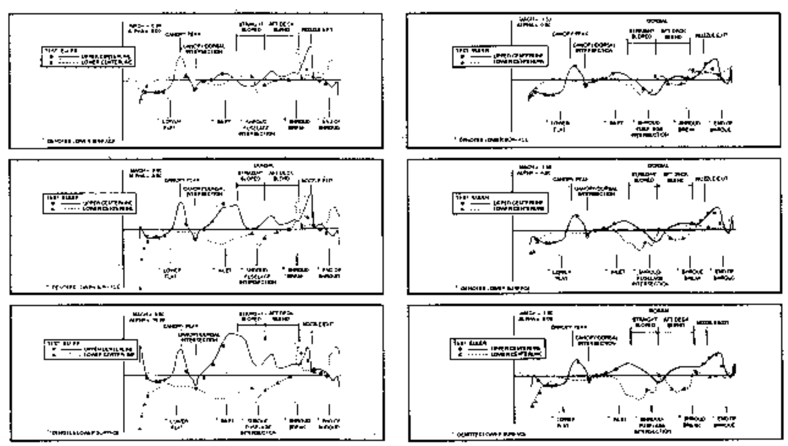

Calculation using AIRPLANE 1987-2005

Airbus A320

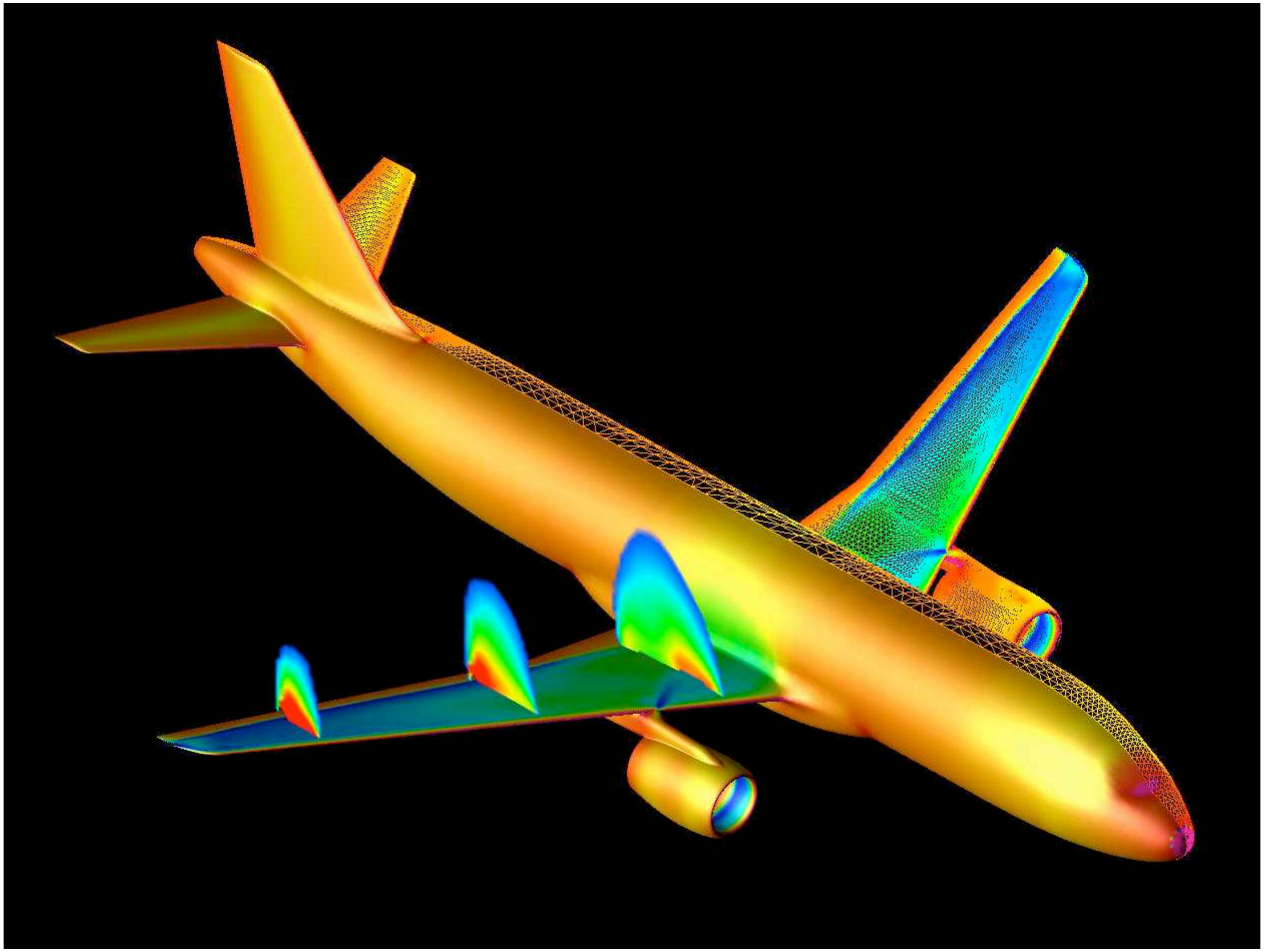

Supersonic Transport Calculation

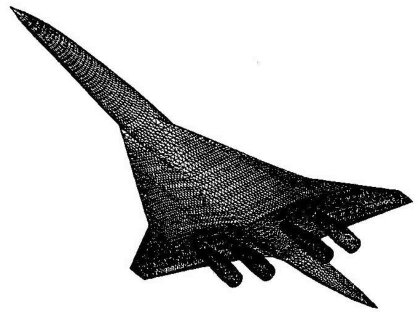

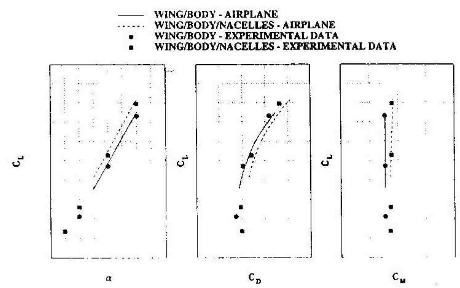

3a: Force Coefficients, Mach 2.1.

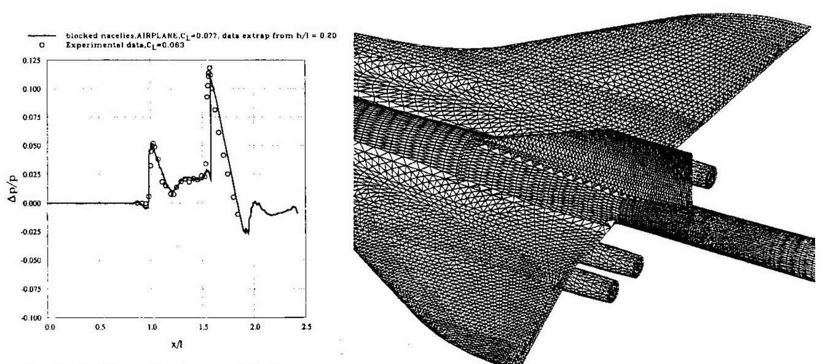

3b: Sonic Boom Prediction, Mach 2.5.

Supersonic Transport

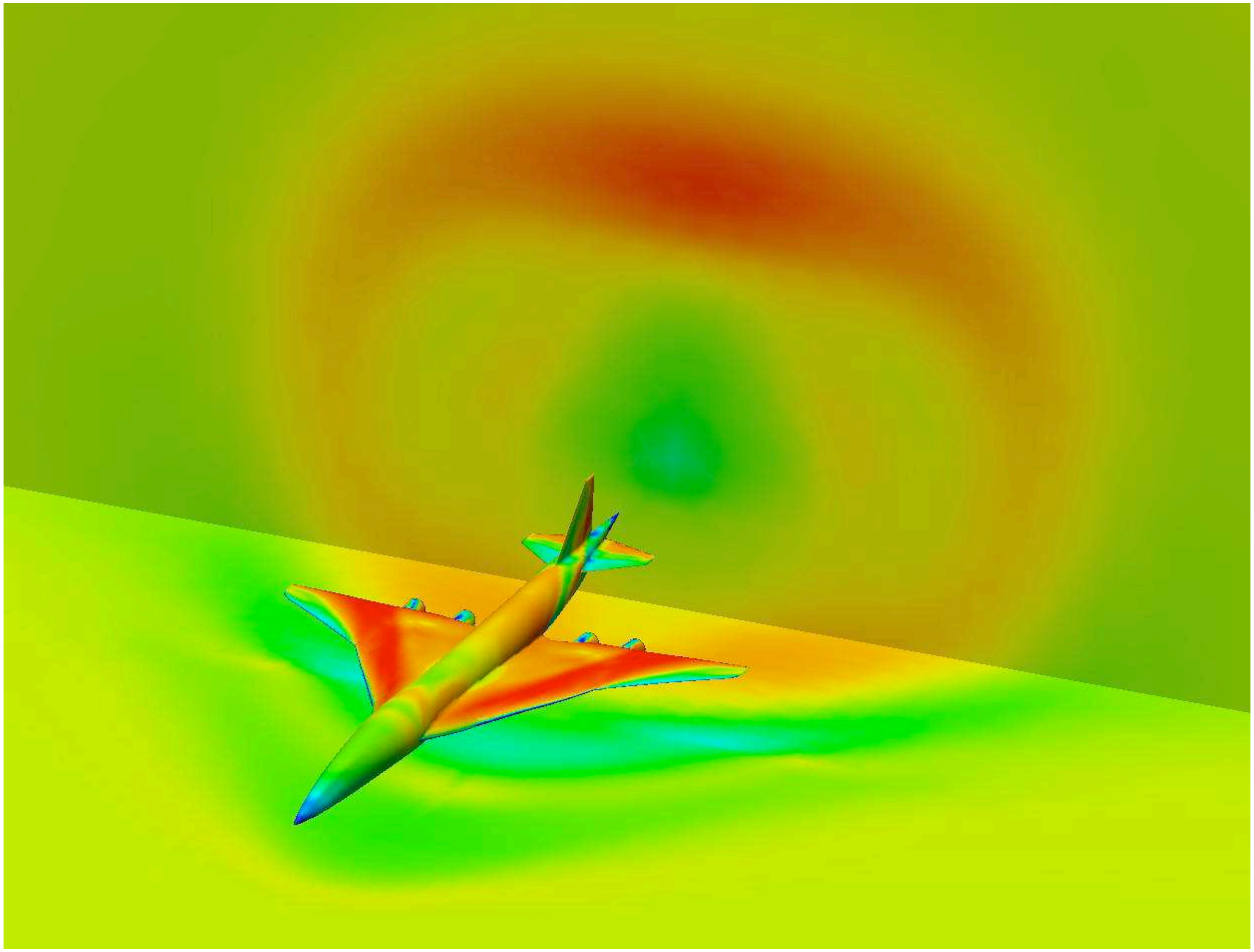

CFD At the Boeing Company

The Impact of CFD on Configuration Lines and Development Wind Tunnel Testing

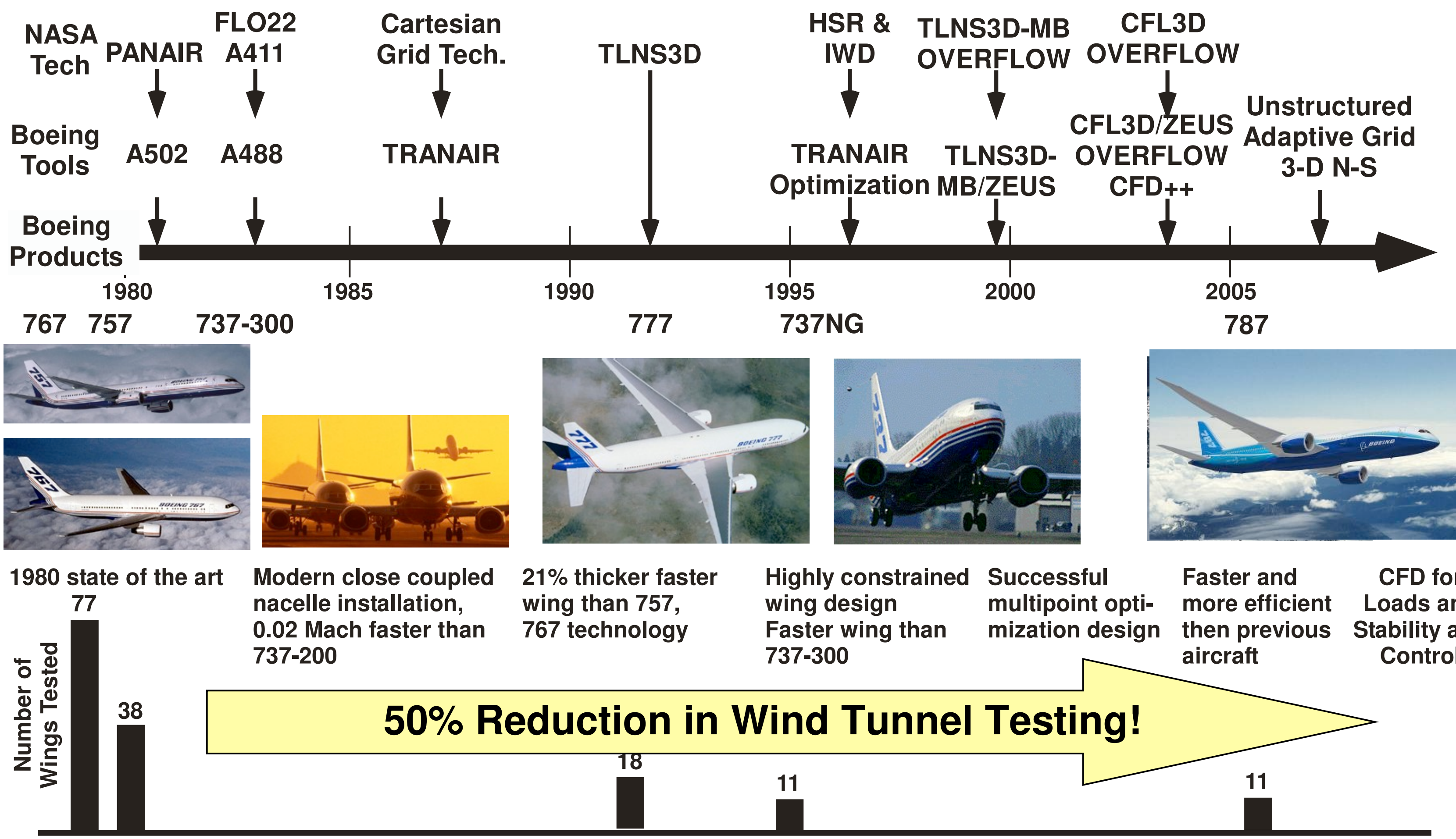

Impact of CFD on the 737-300 Program

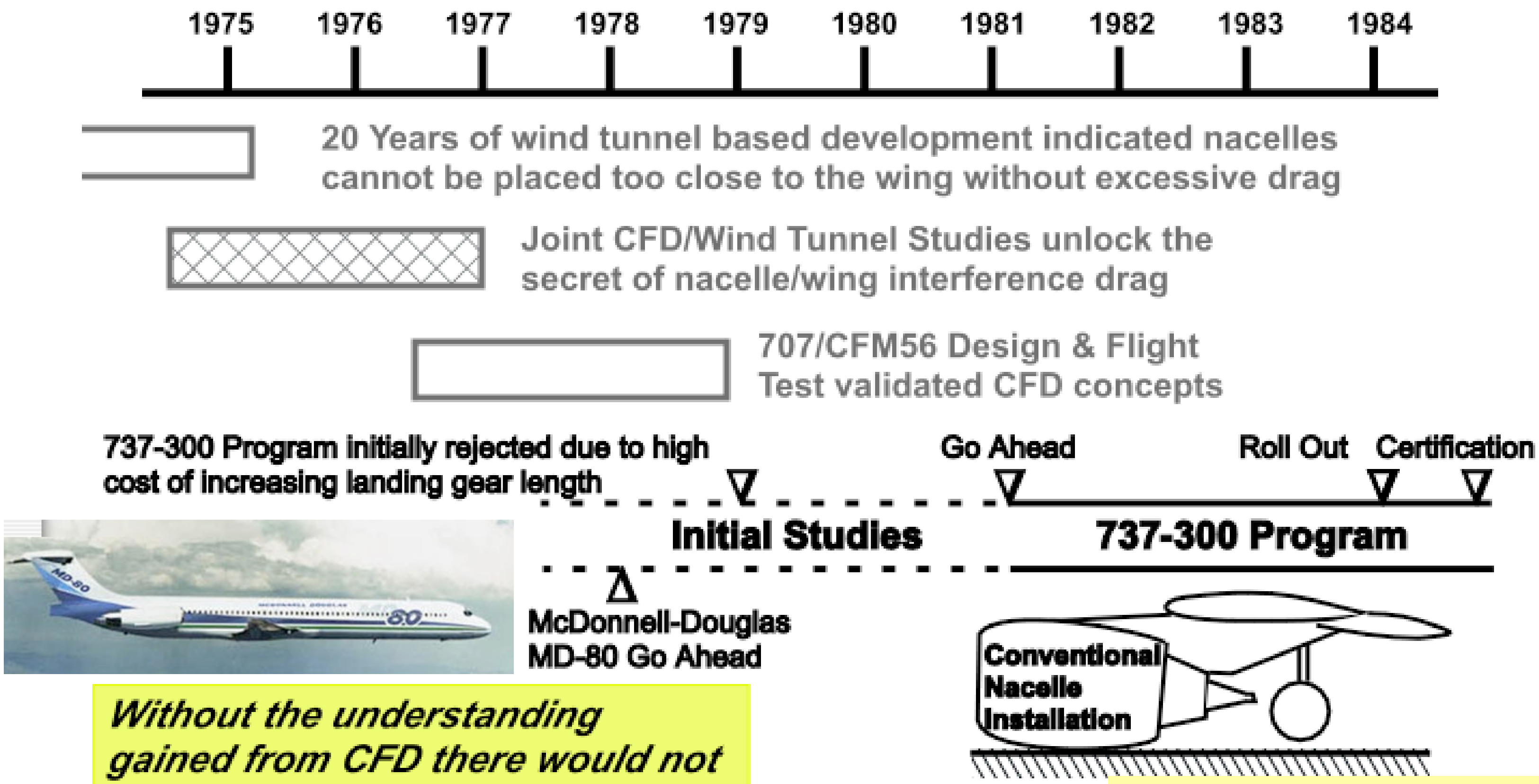

5000+ Additional Sales!

Without the understanding gained from CFD there would not have been a 737-300 Program!

Walt Gillette

Manager, 737 Aerodynamics - then

Vice President, 787 Engineering – retired

CFD Contribution to 787

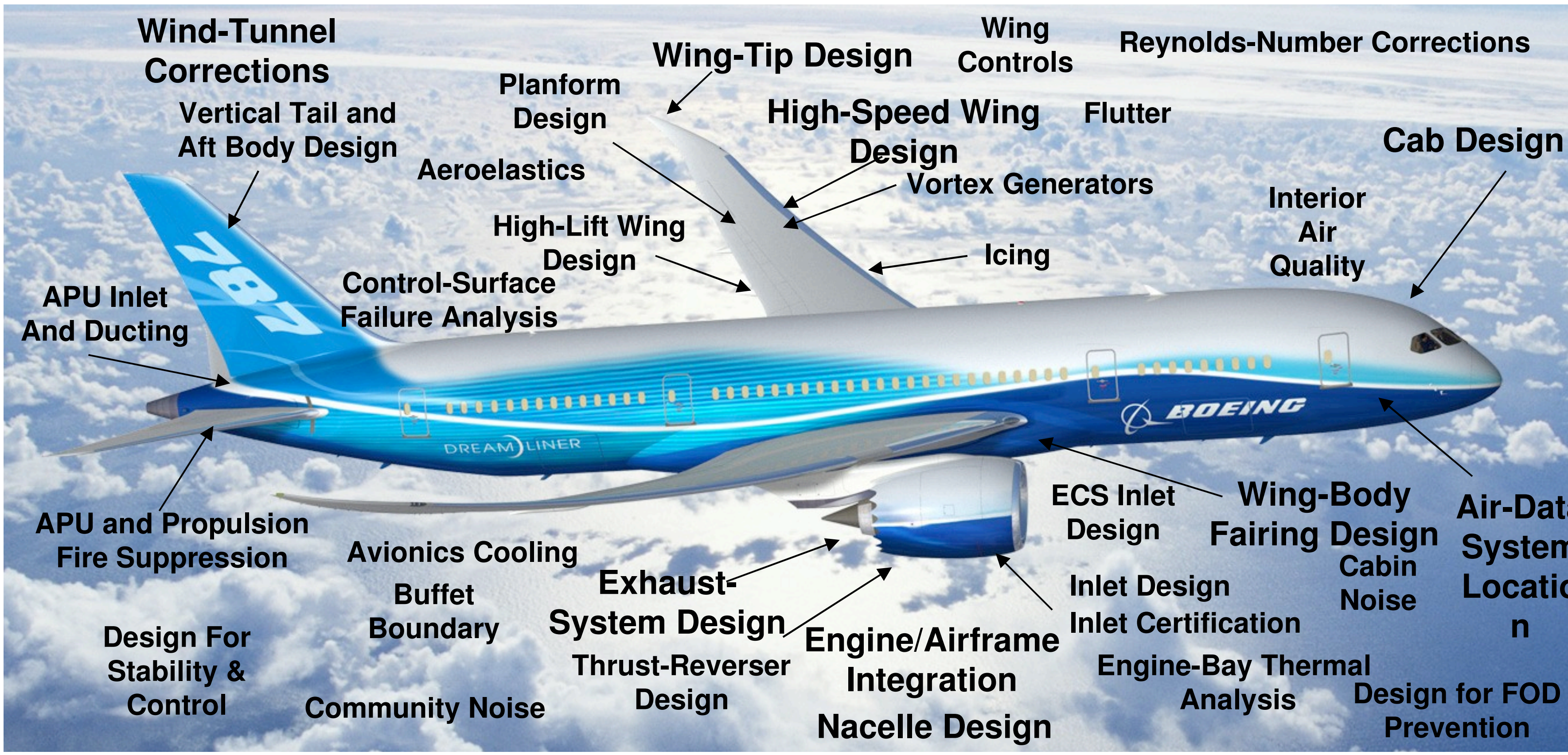

Computational Methods

TRANAIR

- **Full Potential with directly coupled Boundary Layer**
- **Cartesian solution adaptive grid**
- **Drela lag-dissipation turbulence model**
- **Multi-point design/optimization**

Navier-Stokes Codes

- **CFL3D – Structured Multiblock Grid**
- **TLNS3D - Structured Multiblock Grid - Thin Layer**
- **OVERFLOW – Overset Grid**

N-S Turbulence Models

- **S-A Spalart-Allmaras**
- **Menter's k-w SST**

Stable, Packaged Software Solutions – TRANAIR

Scripted and Packaged for a "Standard" Class of Configurations

- **Integral part of the engineering process**
- **Reduces solution flowtime**
- **Improves <u>consistency and repeatability</u> of results**
- **Uses common BCA processes**
- **Improves productivity**

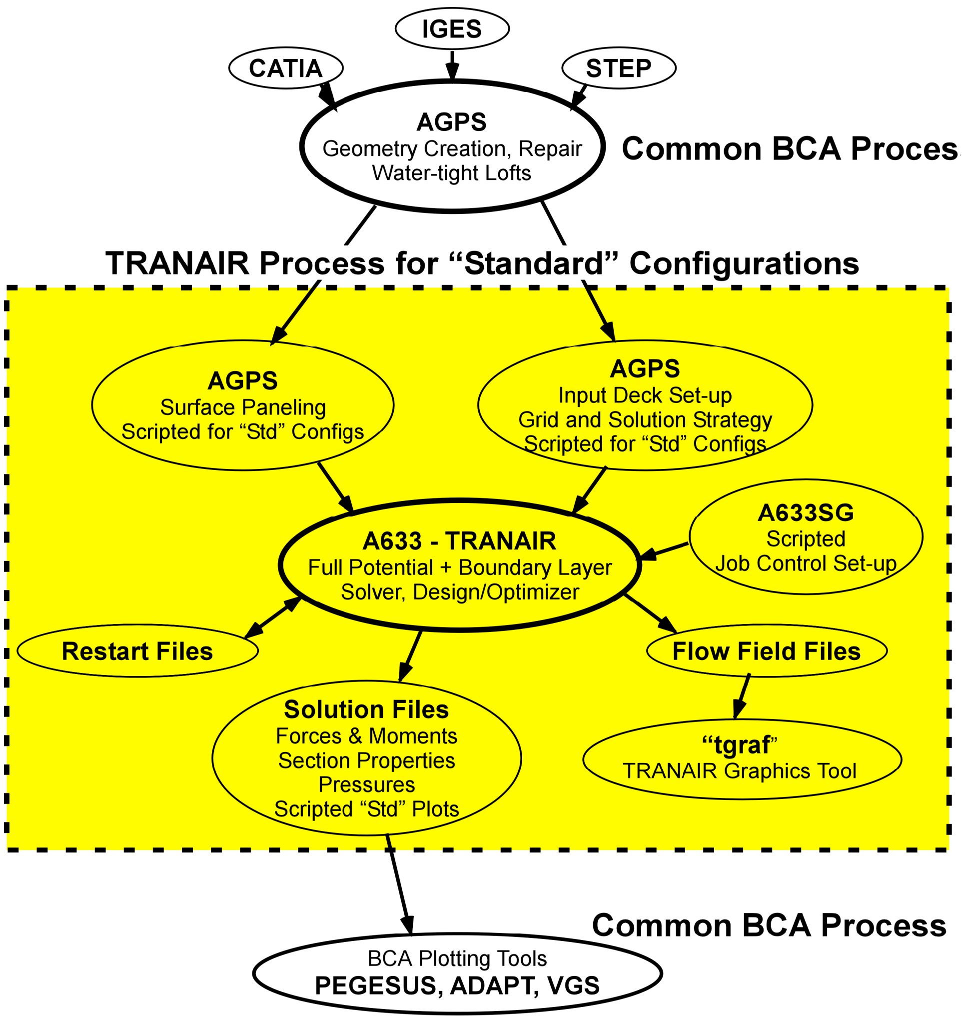

Stable, Packaged Software Solutions – Zeus/CFL3D

Driver for Surface Grid Generation, Volume Grid Generation, Navier-Stokes Analysis, and Post-processing

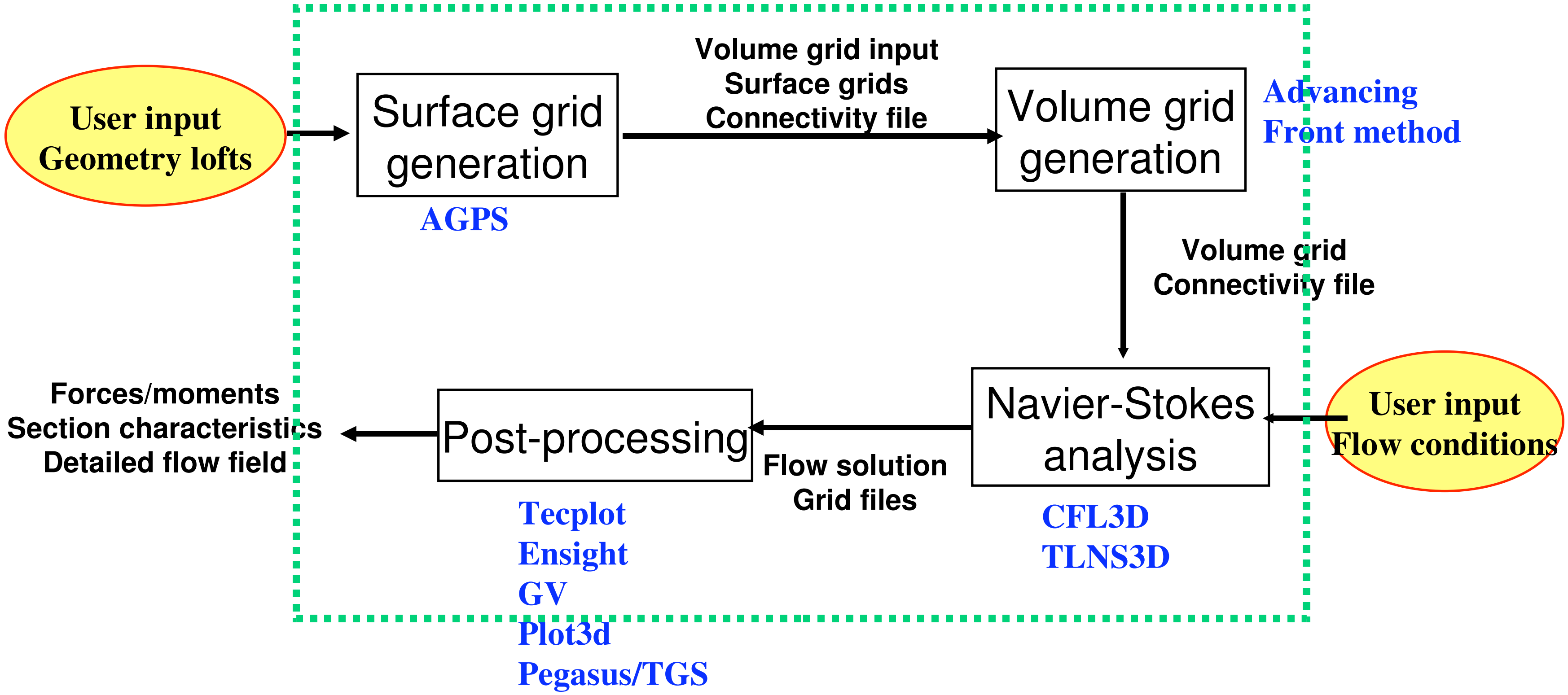

Must be able to do CFD for Full Flight Envelope

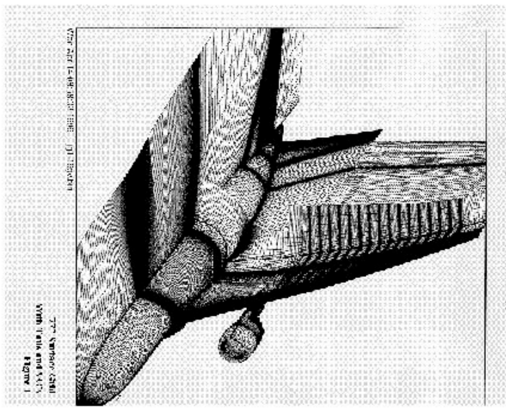

Computational Simulations of a transport with 16 Vortex Generators per Wing

Effect of Vortex Generators on Pitching Moment at High Mach

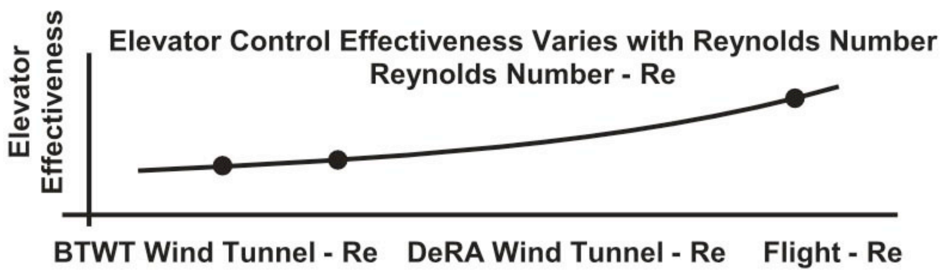

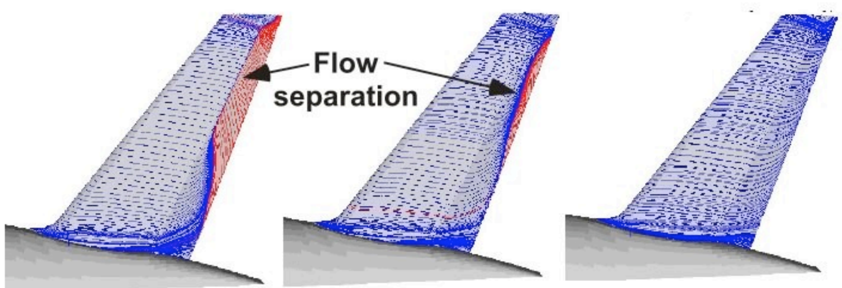

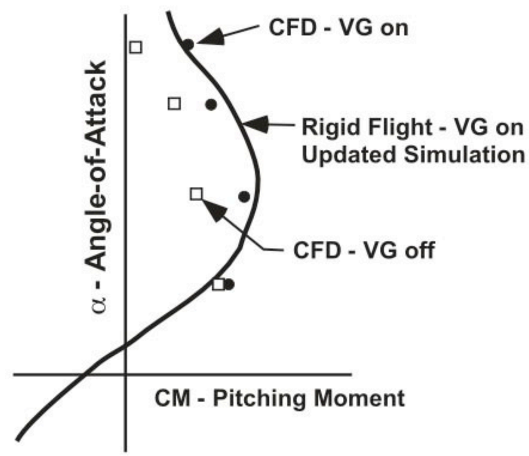

TLNS3DMB - Multi-block Navier-Stokes
21 Million grid points in 79 blocks
60 CPU's - Origin 2000

21st Century Challenge – Aeroacoustic

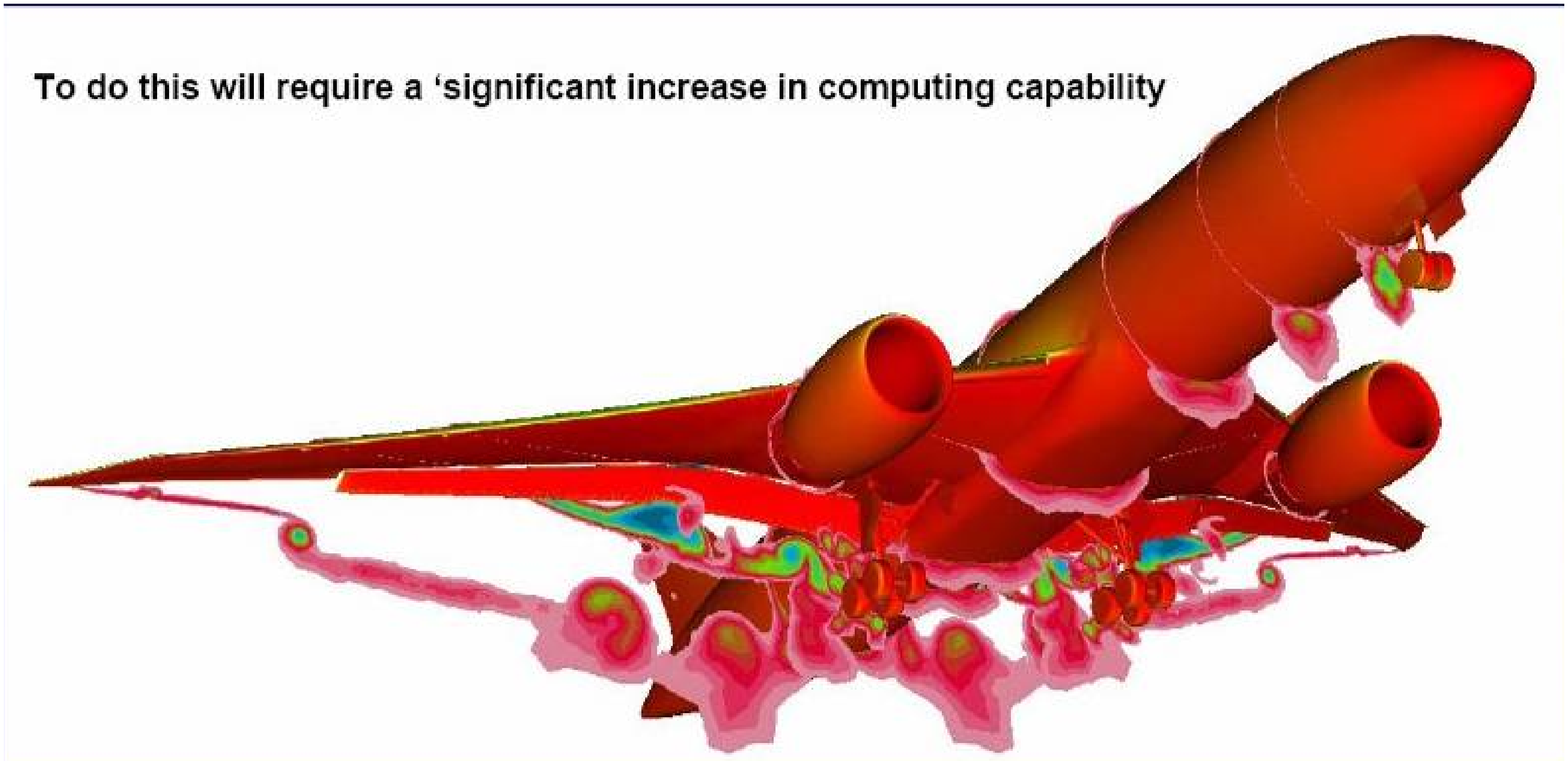

CFD At Airbus and German Aerospace Center (DLR)

Numerical Flow Simulation

- Geometry, flight conditions

- Physical model, governing equations

$$\frac{\partial}{\partial t}\int_V \vec{W}\,dV = -\oint_{\partial V} \vec{F}(\vec{W})\cdot\vec{n}\,dO$$

- Discretization

- Numerical solution

- Flow visualization

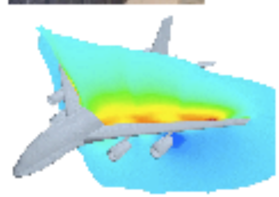

- Aerodynamic data

$C_L = 0.5$, C_D: 0.025, C_M: -0.08

5 + 2
integral equations

10 - 50 million
grid points/ volumes

50 - 350 million
non-linear equations / flow variables

3 - 30
aerodynamic coefficients

Problem: Quality ⇔ Accuracy ⇔ Problem Size ⇔ Time/Costs

CFD Development for Aircraft Applications

MEGAFLOW / MEGADESIGN
- National CFD Initiative (since 1995)

Development & validation of a national CFD software for complete aircraft applications which

- allows computational aerodynamic analysis for 3D complex configurations at cruise, high-lift & off-design conditions
- builds the basis for shape optimization and multidisciplinary simulation
- establishes numerical flow simulation as a routinely used tool at DLR and in German aircraft industry
- serves as a development platform for universities

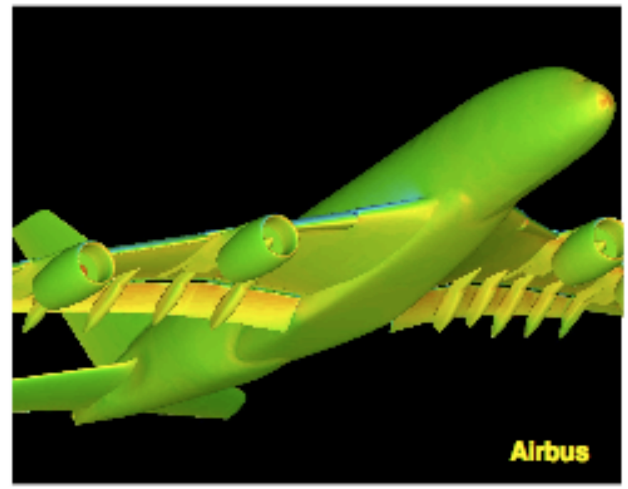

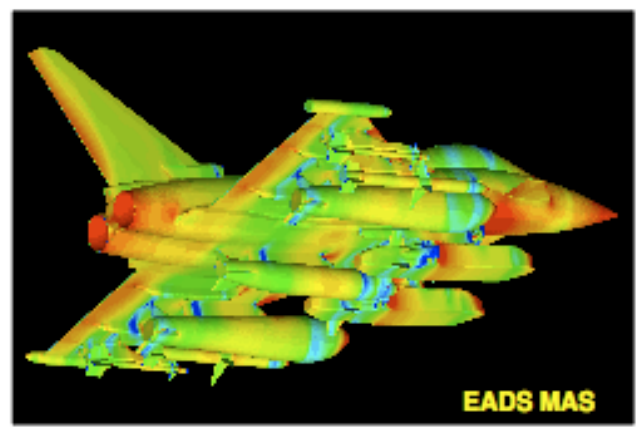

Block-Structured RANS Capability FLOWer

Efficient simulation tool for configurations of moderate complexity

- advanced turbulence and transition models (RSM, DES)
- state-of-the-art algorithms
  - baseline: JST scheme, multigrid
  - robust integration of RSM (DDADI)
- chimera technique for moving bodies
- fluid / structure coupling
- design option (inverse design, adjoint)

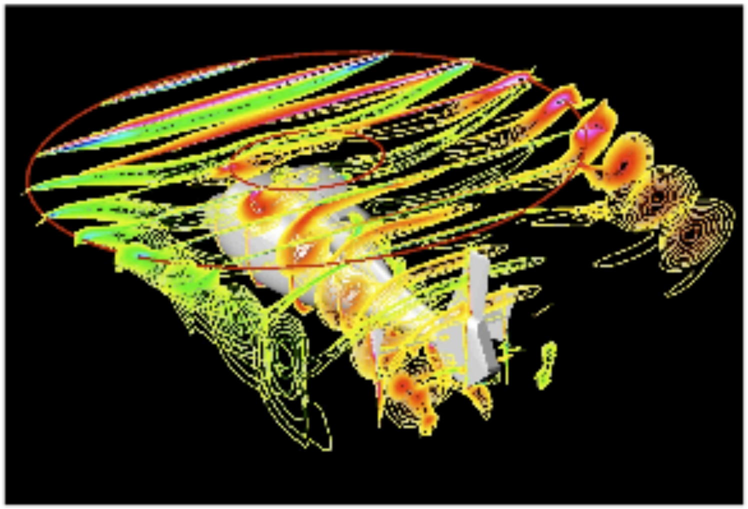

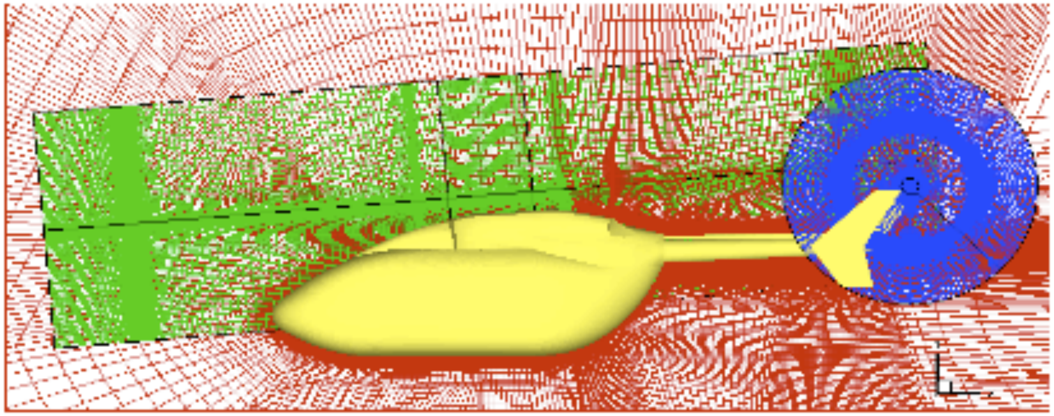

FLOWer-Code

- Fortran
- portable code
- parallelization based on MPI

Unstructured RANS Capability TAU

Tool for complex configurations

- hybrid meshes, cell vertex / cell centered
- high-level turbulence & transition models (RSM, DES, linear stability methods)
- state-of-the-art algorithms (JST, multigrid, …)
- local mesh adaptation
- chimera technique
- fluid / structure coupling
- continuous/discrete adjoint
- extensions to hypersonic flows

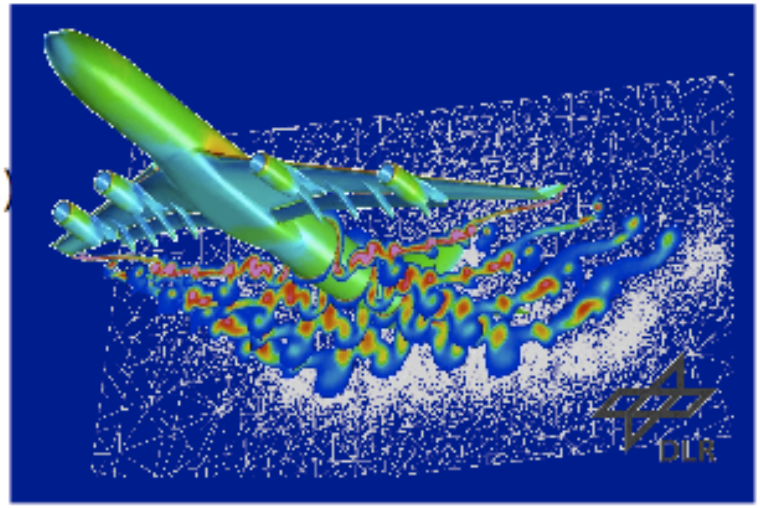

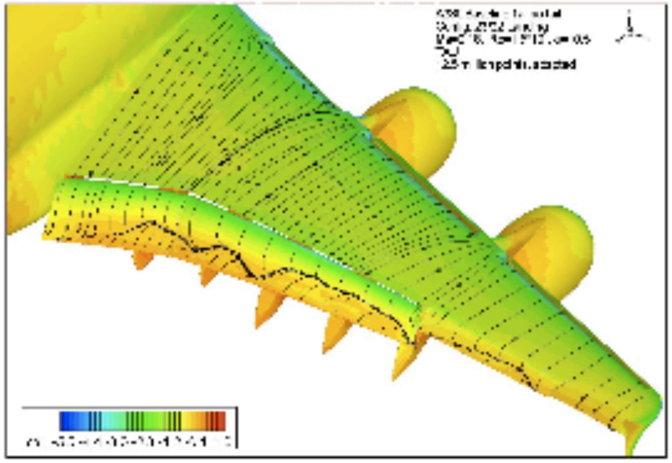

TAU-Code

- unstructured database
- C-code, Python
- portable code, optimized for cache hardware
- high performance on parallel computer

Mesh Generation

Tools

- structured grids
  - *DLR MegaCads*
  - *ICEM-Hexa*
- unstructured grids
  - *CENTAUR,*
  - *UK SOLAR mesher*
  - *EADS-M mesher*
- structured/unstructured grids
  - *DLR MegaCads*

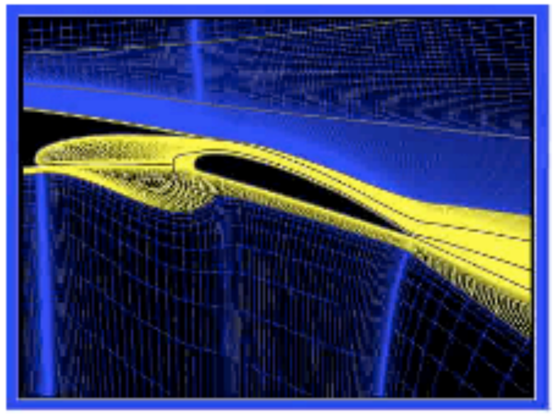

MegaCads

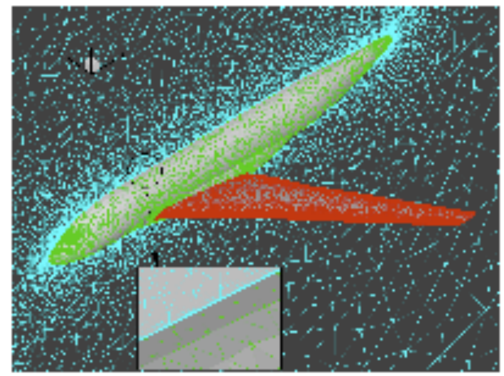

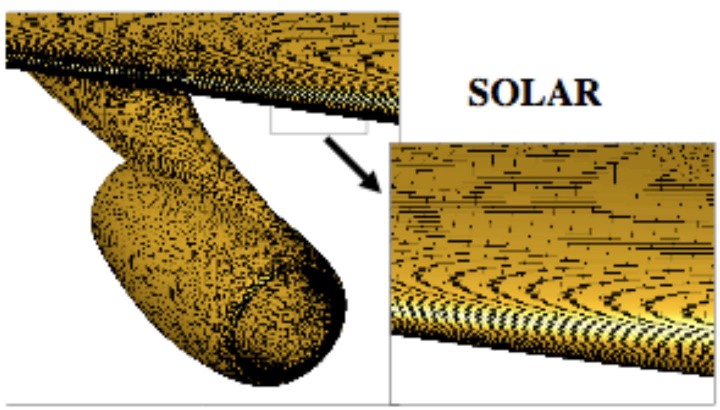

SOLAR

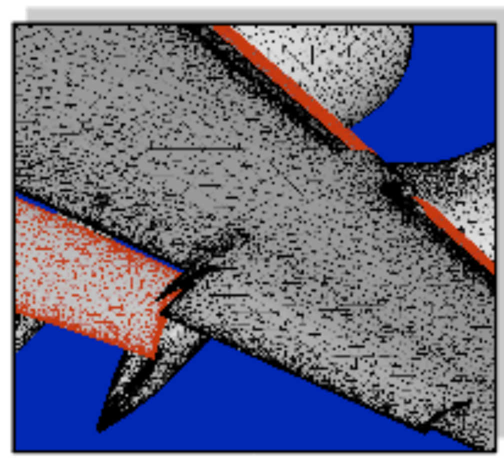

Centaur

Numerical Flow Simulation

Relation CFD / wind tunnel

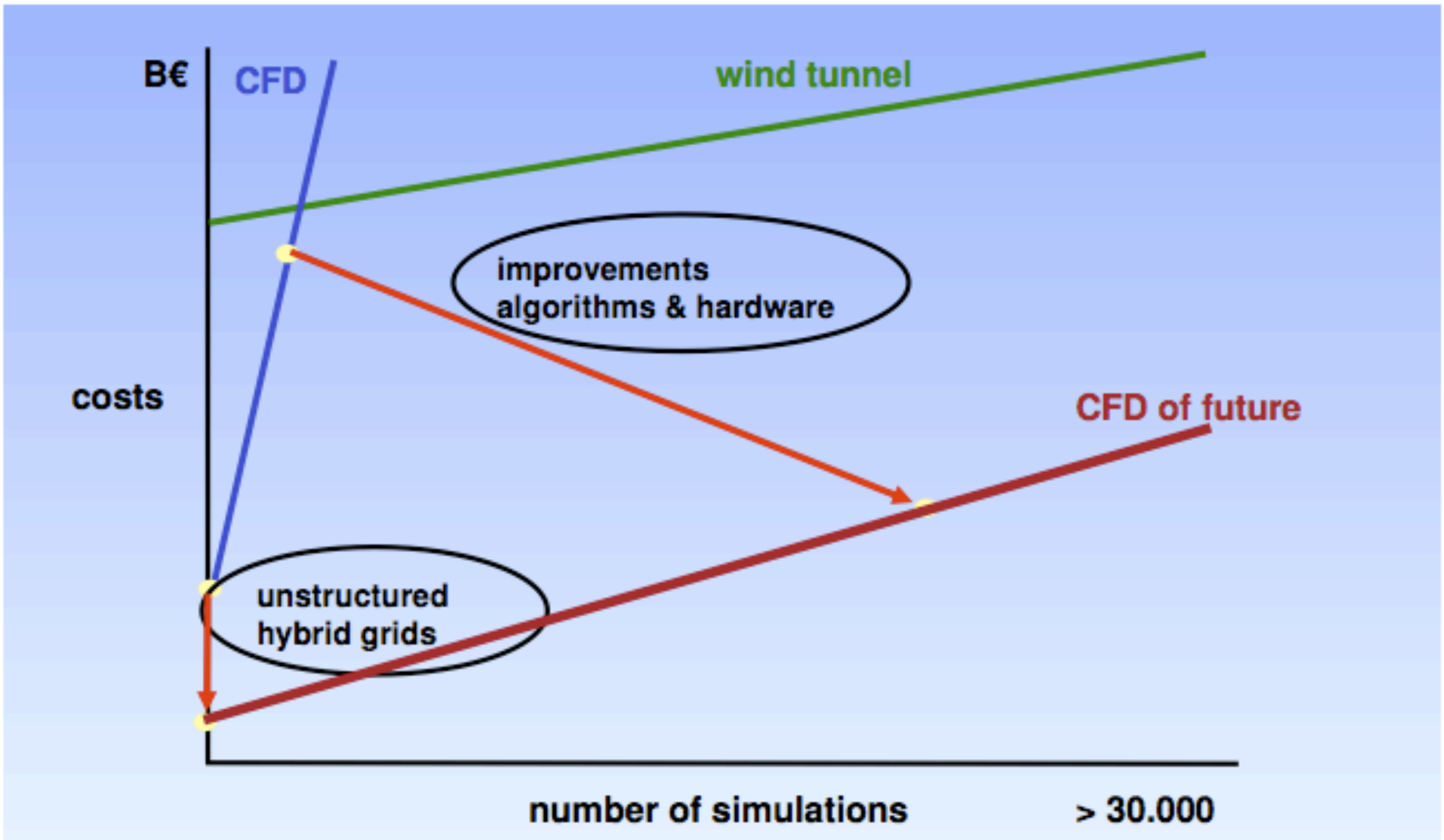

✈ **CFD cost effective alternative**

Numerical Flow Simulation

Cruise Configuration

Influence of Mach number and incidence

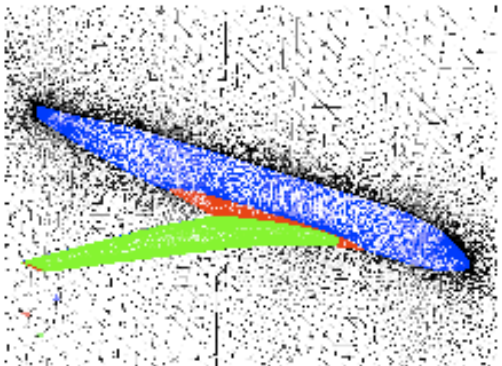

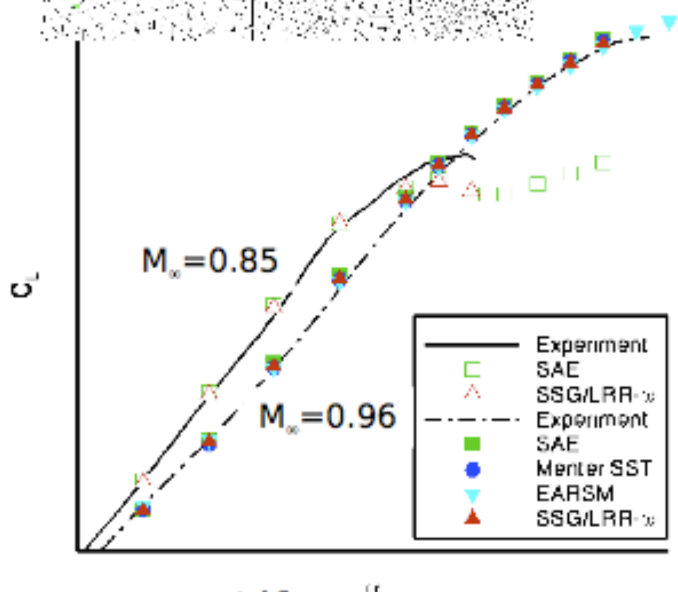

Lift

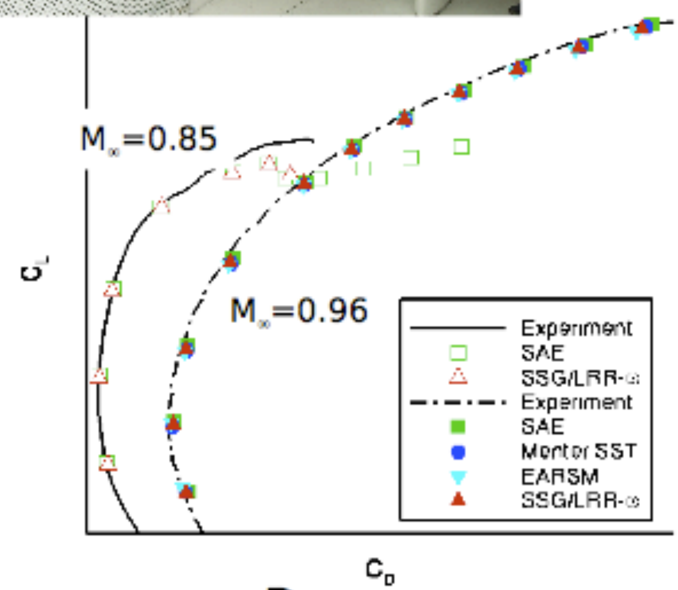

Drag

Aircraft in High Lift Configuration

Effect of nacelle strakes on civil transport configuration

Aircraft in High Lift Configuration

Effect of nacelle strakes on civil transport configuration

- **detailed CFD investigation using CFD (DLR TAU-Code)**

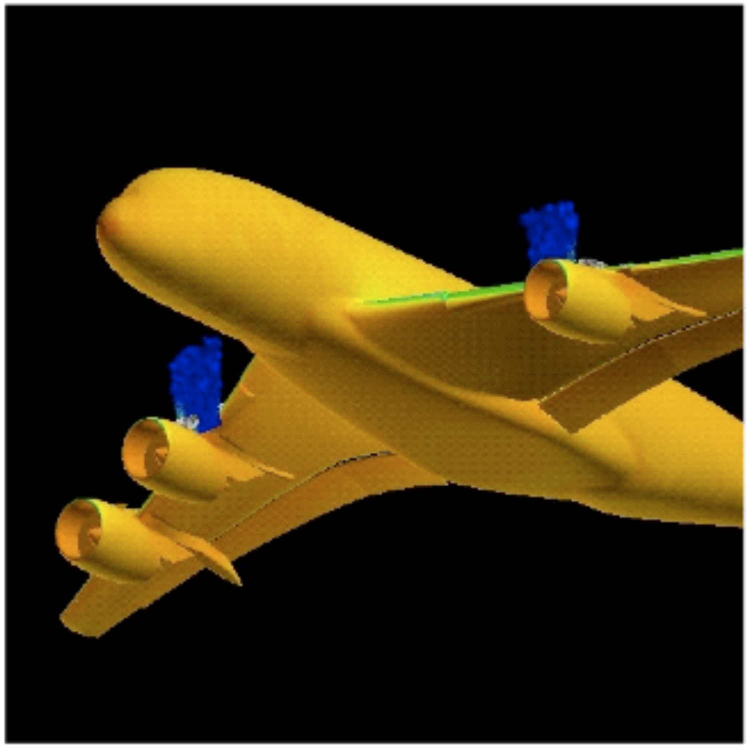

hybrid grid: 17 million points, 3x adapted

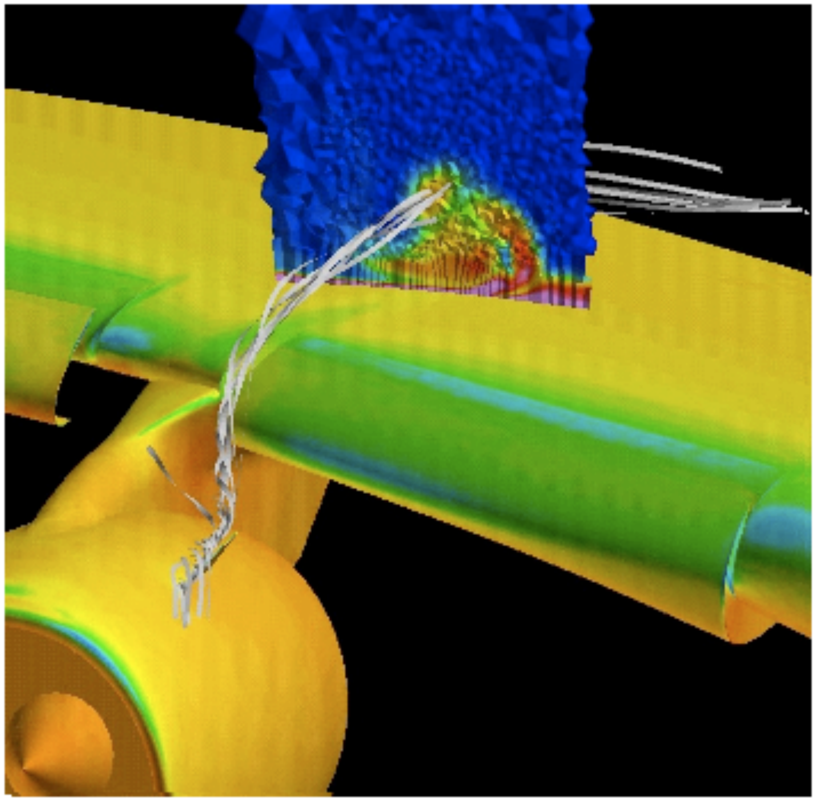

M=0.18. Re=3x10^6

Fluid-Structure Coupling, Cruise

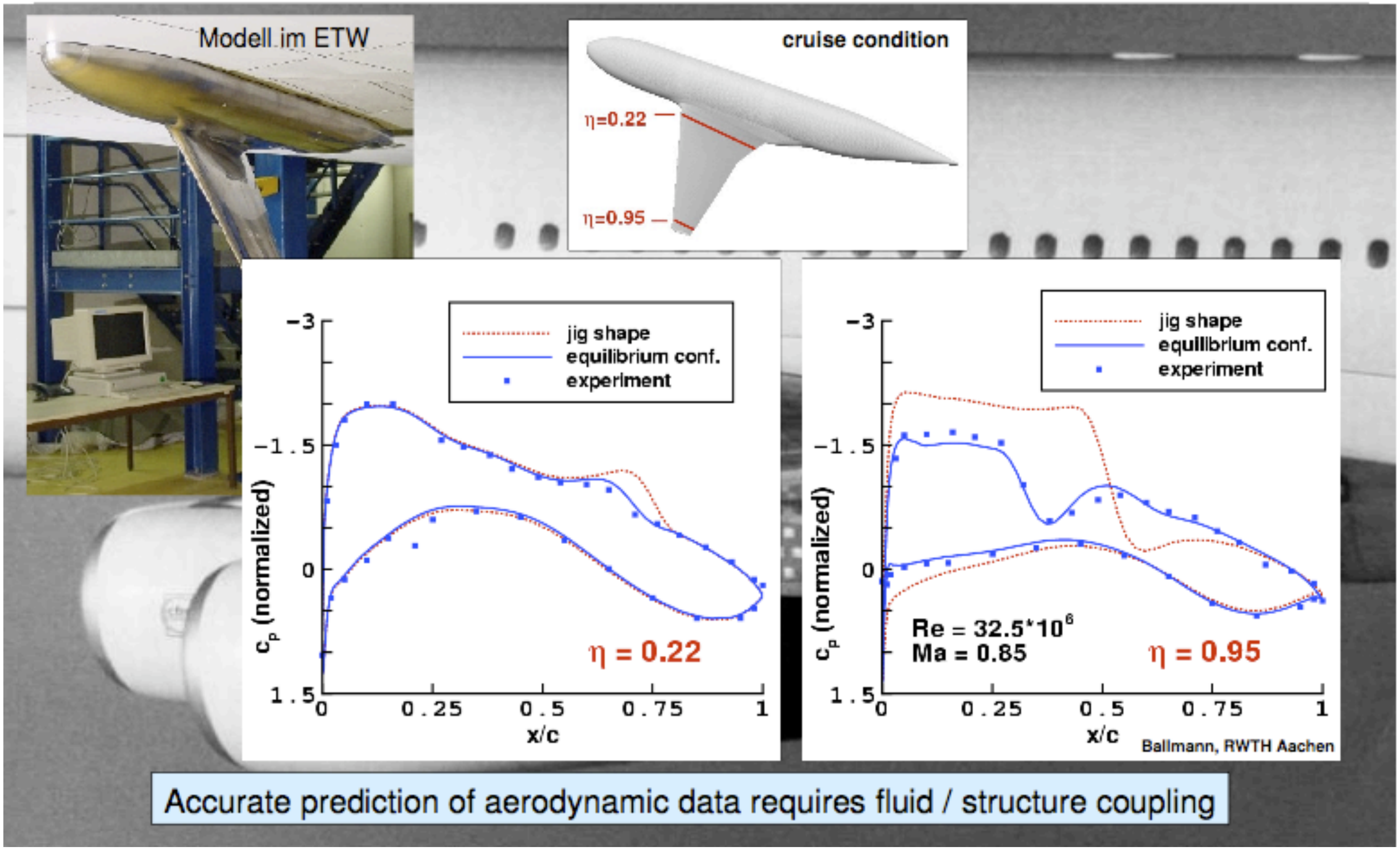

Multidisciplinary Optimization

Shape optimization – Key technology for future product design

Where are we now ?

- pure aerodynamic optimization

  with moderate geometrical complexity and limited number of design variables

What next

- multi-disciplinary optimization
- coupling between aerodynamics structures, propulsion, flight mechanics, aero-acoustics
- large # of design variables
- goals: range improvement, noise reduction, ..
- but: significant higher wall clock time

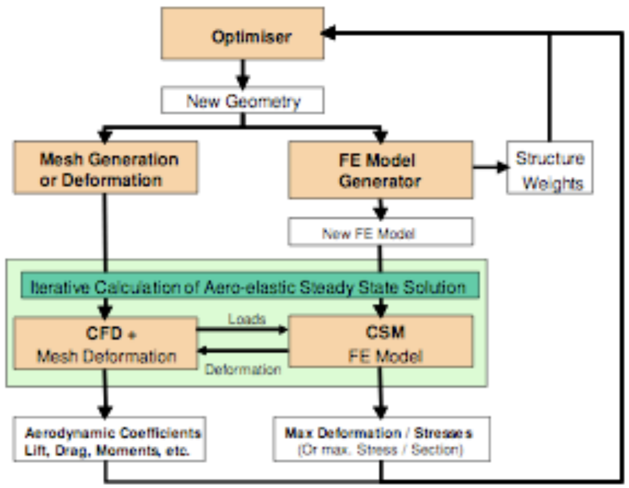

aero/structure optimization

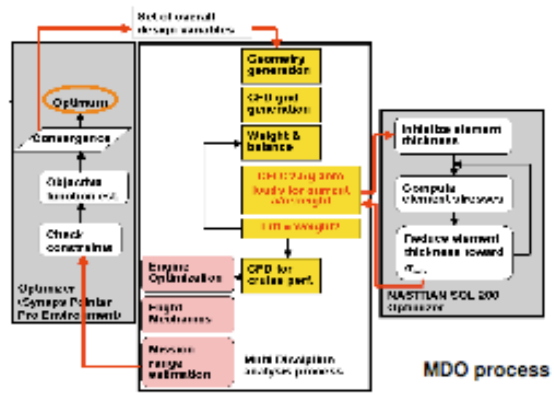

MDO process

Where We Are.. And What Next..

Where We are

- Worldwide commercial and government codes based on algorithms developed in the 80s and 90s
- Can handle complex geometry but limited to 2nd order accuracy
- Can not handle turbulence without modeling
- Unsteady simulations very expensive, and questions over accuracy remain

What Next?

- High order methods seem to offer a route to resolving smaller physical scales without modeling

Introduction of High Order Methods

Higher Order Methods (DG,SV,SD)

- Small numerical dissipation
- Less numerical dispersion
- Unstructured grids
- CPU efficient/easy to parallelize
- Not memory intensive
- Easy to program, universal construction by placing unknown points in a geometrical similar manner
- SD attains a simpler form and higher efficiency than DG and SV.
- Flexible (grid-independence, hp adaptation, moving boundary, deformable grid)

History of Spectral Difference Method

Two early papers on SD method

- D. A. Kopriva and J. H. Kolias, A conservative staggered-grid chebyshev multidomain method for compressible flows. J. Comput. Phys. 125 (1996), p. 244 Structured staggered grid
- Yen Liu , Marcel Vinokur , Z. J. Wang, Spectral difference method for unstructured grids I: basic formulation, Journal of Computational Physics, v.216 p.780-801,2006. Unstructured multivariate formulation

Our papers on SD method

- Wang, Z.J., Liu, Y., May, G., Jameson, A.: "Spectral Difference Method for Unstructured Grids II: Extension to the Euler Equations" , J. Sci. Comput. 32 (1) pp. 54-71, July, 2007. Extension to Euler equations
- C. Liang, S. Premasuthan, A. Jameson, "High-order accurate simulation of flow past two side-by-side cylinders with Spectral Difference method", 2009, vol 87, pp. 812-817, Journal of Computers and Structures. Extension to 2D viscous flow on quadrilateral elements
- C. Liang, A. Jameson and Z. J. Wang, "Spectral Difference method for two-dimensional compressible flow on unstructured grids with mixed elements", Journal of Computational Physics, vol 228, pp 2847-2858, 2009. Extension to 2D viscous flow on mixed elements

Development of SD method in Stanford

- 2D quadrilateral/triangular element
- 3D hexahedral elements
- Raviart-Thomas elements
- Mixed elements
- 4th-order and higher on unstructured grids
- Implicit LU-SGS time stepping
- P-multigrid method
- Moving and deforming grids
- Fluid structure interaction
- Adpative mesh refinement
- Artificial viscosity for shock capturing
- Parallelization (MeTis/MPI) of 3D code

Spectral Difference Method

Triangular, Quadrilateral, and Mixed Elements

Triangular Element

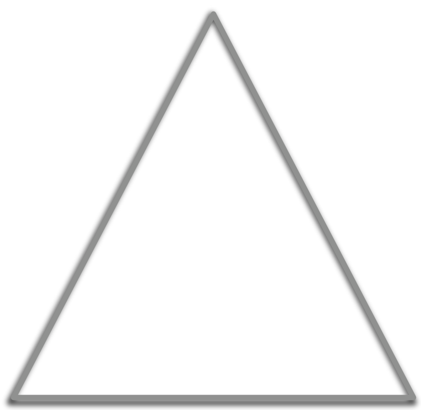

Raviart-Thomas

Mixed Element

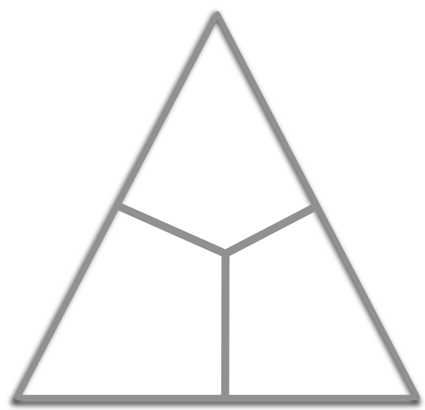

Triangles Can Be Split into Quads and Solved as Quad Elements

Quadrilateral Element

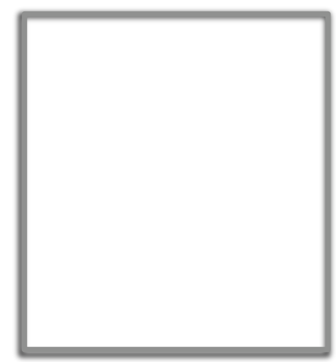

Tensor Inner Product of 1D Polynomials

SD With Triangular Elements using Raviart-Thomas Basis Functions

Triangular Element

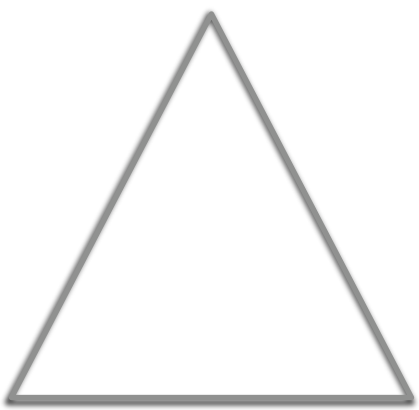

Raviart-Thomas

SD With Triangular Elements using Raviart-Thomas

- Low-order Raviart-Thomas elements used in finite element schemes

- High-order Raviart-Thomas elements rarely used in practice

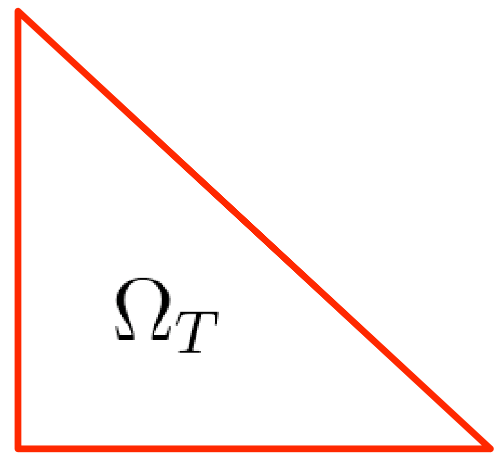

$$\mathbf{RT}_k(\Omega_T) = (\mathbf{P}_k)^2 + \binom{r}{s}\overline{\mathbf{P}}_k \subset (\mathbf{P}_{k+1})^2$$

$$\dim[\mathbf{RT}_k(\Omega_T)] = (k+1)(k+3)$$

SD With Triangular Elements using Raviart-Thomas

$$\mathbf{RT}_2(\Omega_T) = \Bigg[\begin{pmatrix} 1 \\ 0 \end{pmatrix}, \begin{pmatrix} 0 \\ 1 \end{pmatrix}, \begin{pmatrix} r \\ 0 \end{pmatrix}, \begin{pmatrix} 0 \\ r \end{pmatrix}, \begin{pmatrix} s \\ 0 \end{pmatrix}, \begin{pmatrix} 0 \\ s \end{pmatrix}, \begin{pmatrix} rs \\ 0 \end{pmatrix}, \begin{pmatrix} 0 \\ rs \end{pmatrix}, \begin{pmatrix} s^2 \\ 0 \end{pmatrix}, \begin{pmatrix} 0 \\ s^2 \end{pmatrix}, \begin{pmatrix} r^2 \\ 0 \end{pmatrix}, \begin{pmatrix} 0 \\ r^2 \end{pmatrix}, \begin{pmatrix} sr^2 \\ rs^2 \end{pmatrix}, \begin{pmatrix} rs^2 \\ s^3 \end{pmatrix}, \begin{pmatrix} r^3 \\ sr^2 \end{pmatrix} \Bigg]$$

Example with $k = 2$

SD With Triangular Elements using Raviart-Thomas

$$\boxed{\mathbf{q} \in \mathbf{RT}_k(\Omega_T)}$$

$$\int_{\Omega_T} \mathbf{p} \cdot \mathbf{q} \, \mathrm{d}r \mathrm{d}s \qquad \mathbf{p} \in (\mathbf{P}_{k-1})^2 \qquad k(k+1)$$

$$\mathbf{q} \cdot \mathbf{n} \quad \text{at } k+1 \text{ points per edge} \quad 3(k+1)$$

$k = 1$

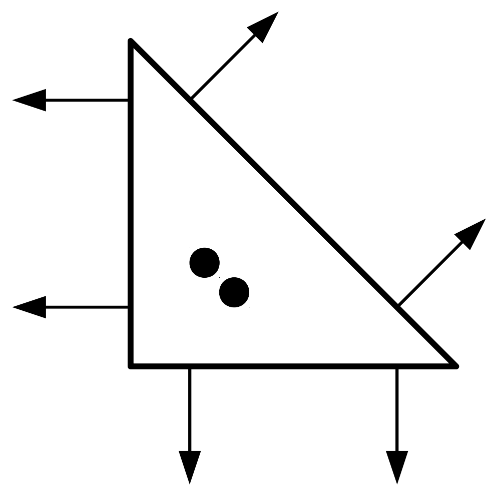

SD With Triangular Elements using Raviart-Thomas

$$\mathbf{q} \in \mathbf{RT}_k(\Omega_T)$$

$$\boxed{\int_{\Omega_T} \mathbf{p} \cdot \mathbf{q} \, \mathrm{d}r\mathrm{d}s \qquad \mathbf{p} \in (\mathbf{P}_{k-1})^2 \qquad k(k+1)}$$

$$\mathbf{q} \cdot \mathbf{n} \quad \text{at } k+1 \text{ points per edge} \quad 3(k+1)$$

$$k = 1$$

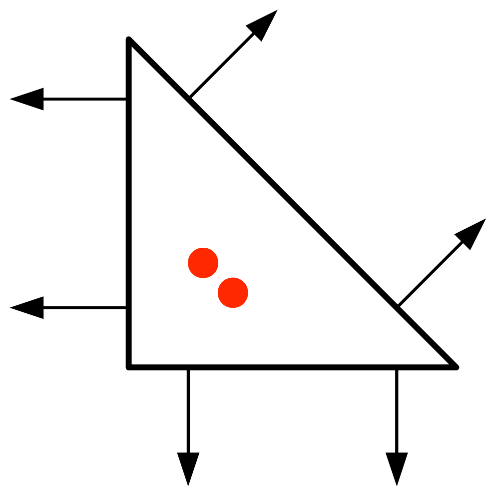

SD With Triangular Elements using Raviart-Thomas

$$\mathbf{q} \in \mathbf{RT}_k(\Omega_T)$$

$$\int_{\Omega_T} \mathbf{p} \cdot \mathbf{q} \, \mathrm{d}r\mathrm{d}s \qquad \mathbf{p} \in (\mathbf{P}_{k-1})^2 \qquad k(k+1)$$

$$\boxed{\mathbf{q} \cdot \mathbf{n} \quad \text{at } k+1 \text{ points per edge} \quad 3(k+1)}$$

$$k = 1$$

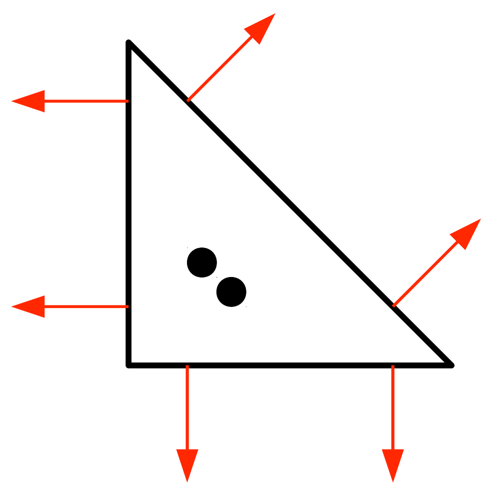

SD Formulation With Quadrilateral Elements

Mixed Element

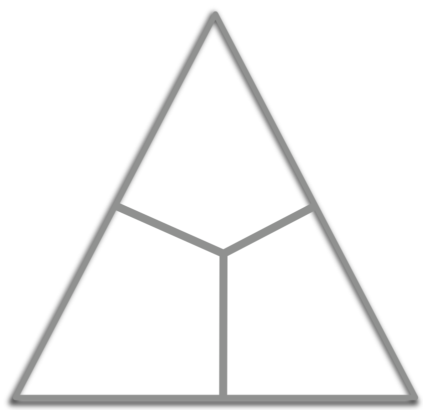

Triangles Can Be Split into Quads and Solved as Quad Elements

Quadrilateral Element

Tensor Inner Product of 1D Polynomials

Affine Mapping for Hexahedral Grid

$$\begin{pmatrix} x \\ y \\ z \end{pmatrix} = \sum_{i=1}^{K} M_i\,(\xi,\eta,\beta)\begin{pmatrix} x_i \\ y_i \\ z_i \end{pmatrix}$$

- Mapping from physical hexahedral grid elements to a standard computational element

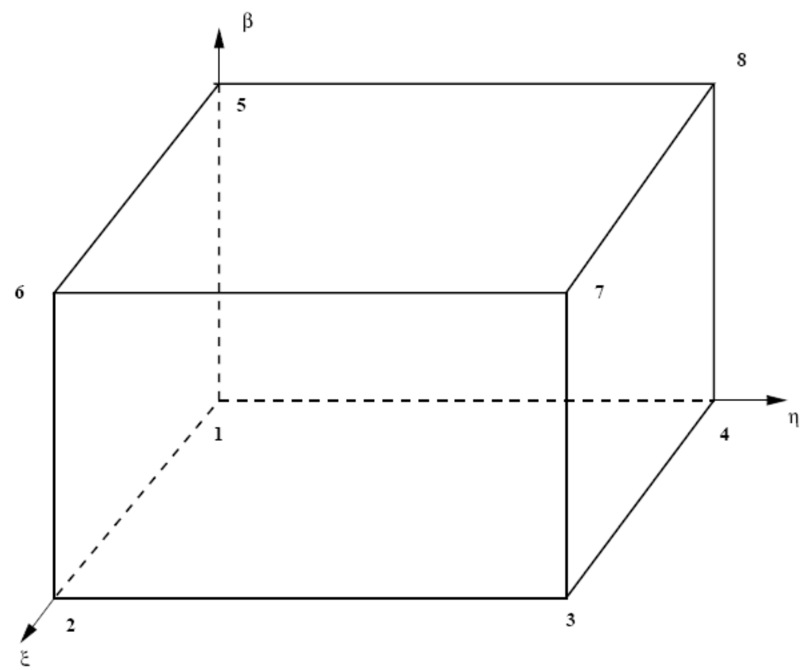

$$(0 \le \xi \le 1,\ 0 \le \eta \le 1 \text{ and } 0 \le \beta \le 1)$$

Flux and Solution Points

- The figure shows one way to locally construct a third-order spectral difference scheme for a grid cell.
- 9 solution points are used.
- 24 flux points are employed.
- The reconstructed field using polynomials is continuous within the cell but discontinuous across the cell boundaries

  - Flux points store F
  - Solution points store Q

$$\frac{\partial Q}{\partial t} + \frac{\partial F}{\partial x} + \frac{\partial G}{\partial y} = 0$$

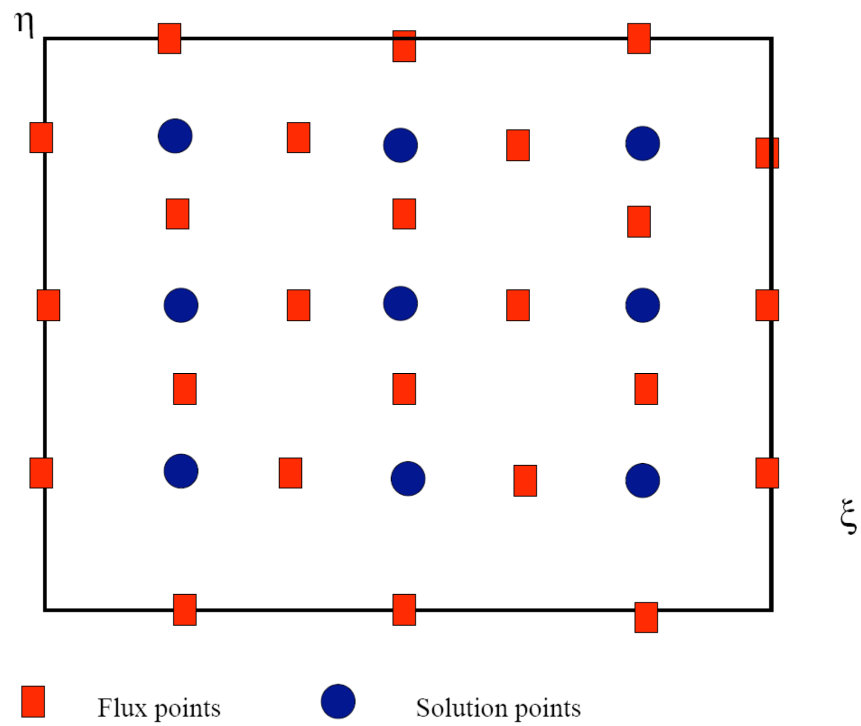

Distribution of Flux and Solution Points

- Solution points are chosen as the Chebyshev points

$$X_s = \frac{1}{2}\left[1 - cos\left(\frac{2s-1}{2N}\cdot\pi\right)\right], s = 1, 2, \cdots, N.$$

- Flux points are chosen as the Legendre-Gauss quadrature points and two end points 0 and 1

$$P_n(\xi) = \frac{2n-1}{n}(2\xi - 1)P_{n-1}(\xi) - \frac{n-1}{n}P_{n-2}(\xi)$$

Flux and Solution Reconstructions

- Using Lagrange Basis to construct polynomials for both the solution and the flux

- Degree N-1 polynomial using solution points

$$h_i(X) = \prod_{s=1, s\neq i}^{N} \left(\frac{X - X_s}{X_i - X_s} \right)$$

- Degree N polynomial using flux points

$$l_{i+1/2}(X) = \prod_{s=0, s\neq i}^{N} \left(\frac{X - X_{s+1/2}}{X_{i+1/2} - X_{s+1/2}} \right)$$

- Reconstructed solution and flux polynomials within an element are written as tensor products of three 1D polynomials

Calculation of Inviscid Flux Derivatives

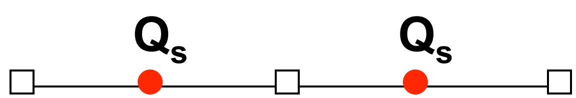

① Given the conservative variables at the solution points, the conservative variables are extrapolated to the flux points

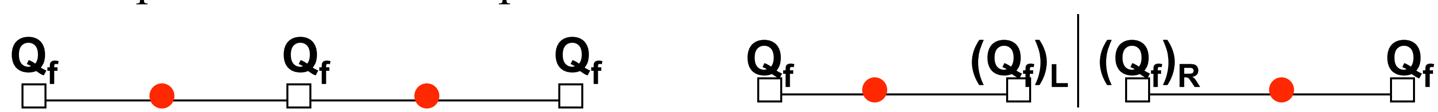

② The inviscid fluxes at the interior flux points are computed

➢ The inviscid fluxes at the element interfaces are computed using a Riemann solver

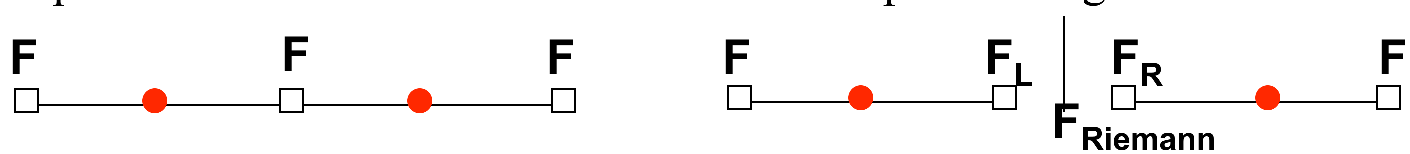

③ The derivative of the fluxes are computed at the solution points

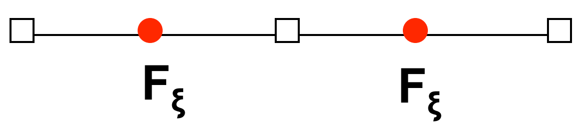

Calculation of Viscous Flux Derivatives

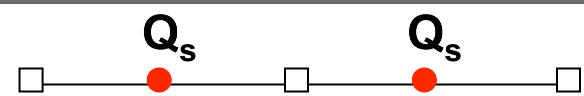

① Given the conservative variables at the solution points, the conservative variables are extrapolated to the flux points

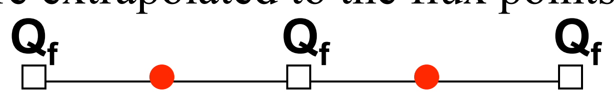

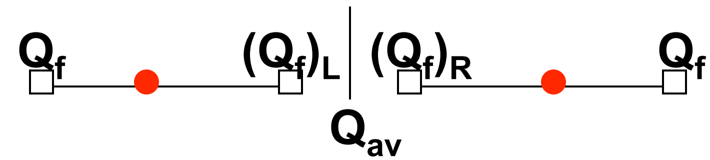

② Calculate the gradient of Q at the solution points from Q at flux points

➢ At flux points on element interfaces, compute the average of left and right values

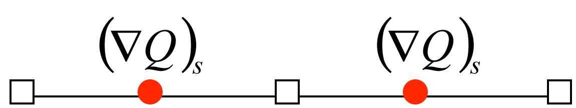

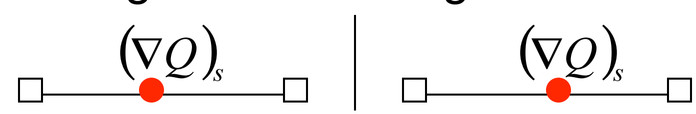

③ Reconstruct the gradient of Q from solution points to flux points

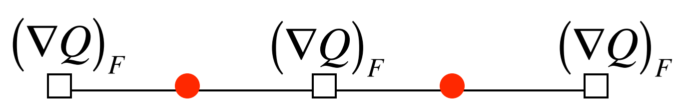

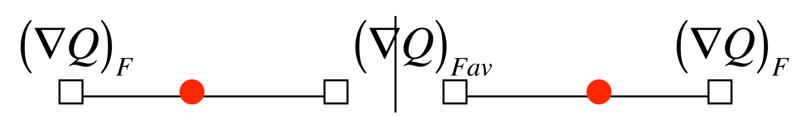

④ Compute viscous fluxes at flux points and then its derivatives at the solution points

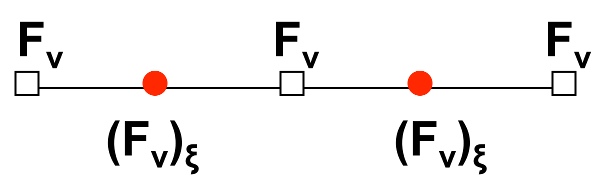

Curved Wall Representation

- M is shape function
- K=4 for 2D linear mapping
- K=8 for 2D quadratic mapping
- K=12 for 2D cubic mapping

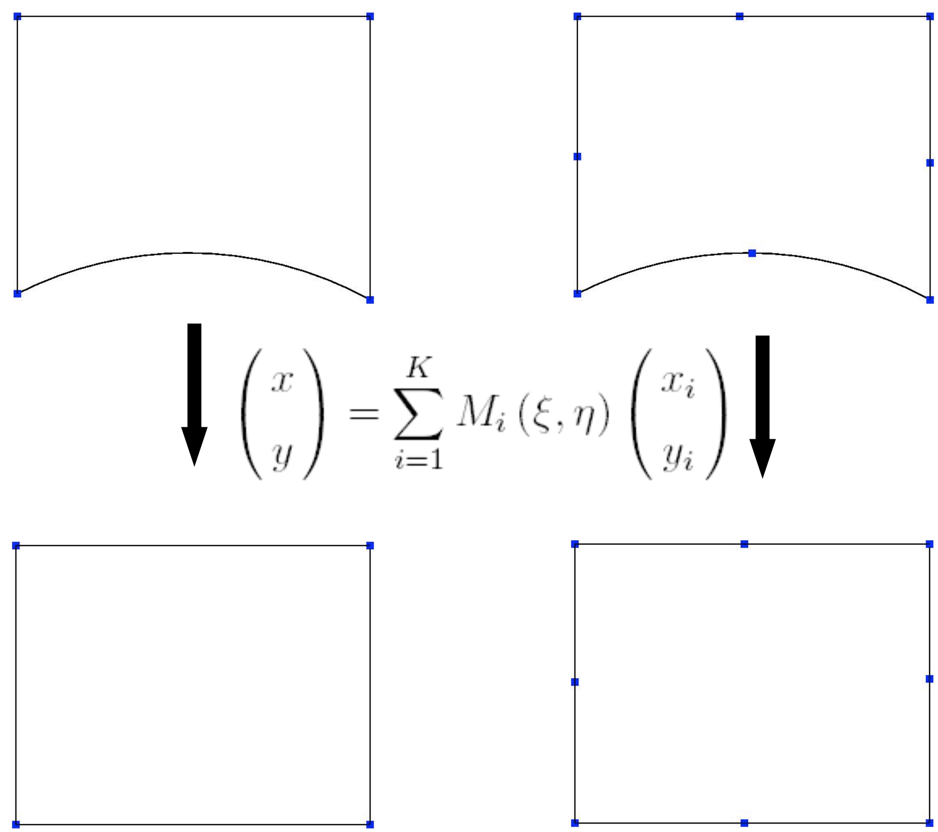

$$\begin{pmatrix} x \\ y \end{pmatrix} = \sum_{i=1}^{K} M_i(\xi, \eta) \begin{pmatrix} x_i \\ y_i \end{pmatrix}$$

Effect of High Order Curved Wall

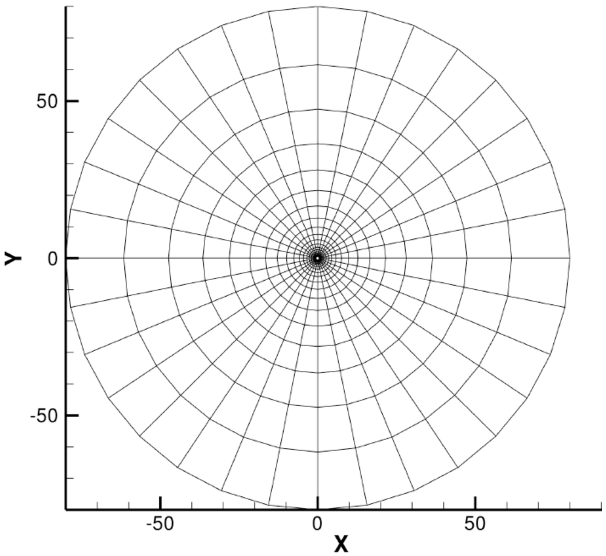

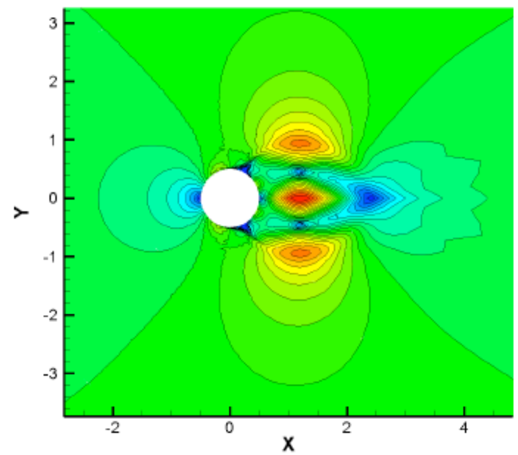

(a) linear wall boundary

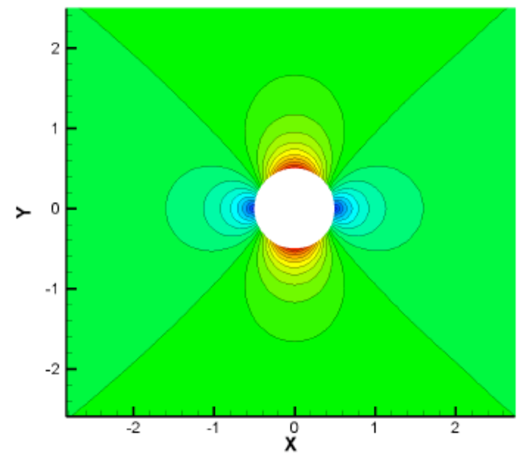

(b) cubic wall boundary

4th-order SD method on a grid with 32x32 cells

- Free stream Mach = 0.2
- Inviscid Euler solver

Effect of Inter-Element Flux Formulas on Cd

Riemann	order	cell no.	Wall	Mach	$\Delta_t u_\infty / D$	C_d
CUSP[8]	4th	640	quadratic	0.2	2e-4	-1.86e-5
AUSM[10]	4th	640	quadratic	0.2	2e-4	-4.39e-5
Roe[16]	4th	640	quadratic	0.2	2e-4	-1.03e-5
Vector split[20]	4th	640	quadratic	0.2	2e-4	-1.18e-5
Rusanov[17]	4th	640	quadratic	0.2	2e-4	-8.8e-6

Numerical Validation

Compressible Taylor-Couette Flow

➢ Mach =0.5, Re=10, isothermal for inner cylinder and adiabatic wall for outer cylinder

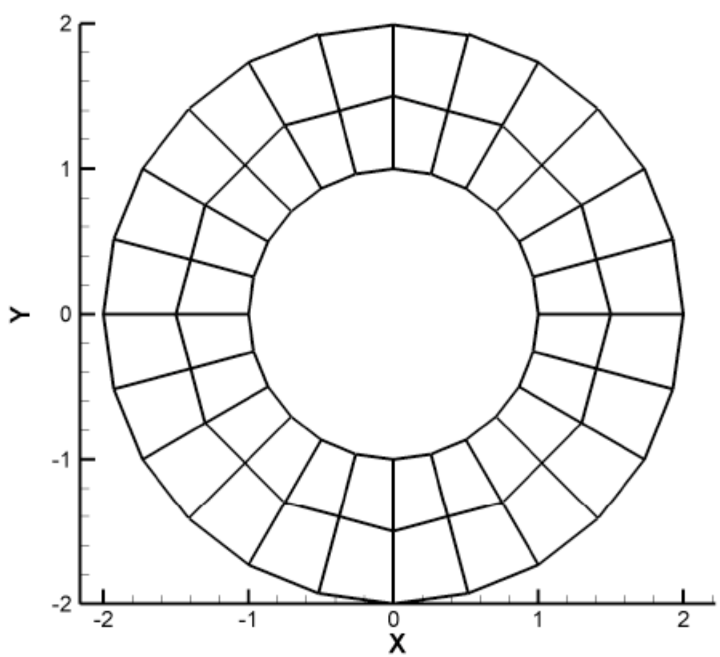

(a) Grid

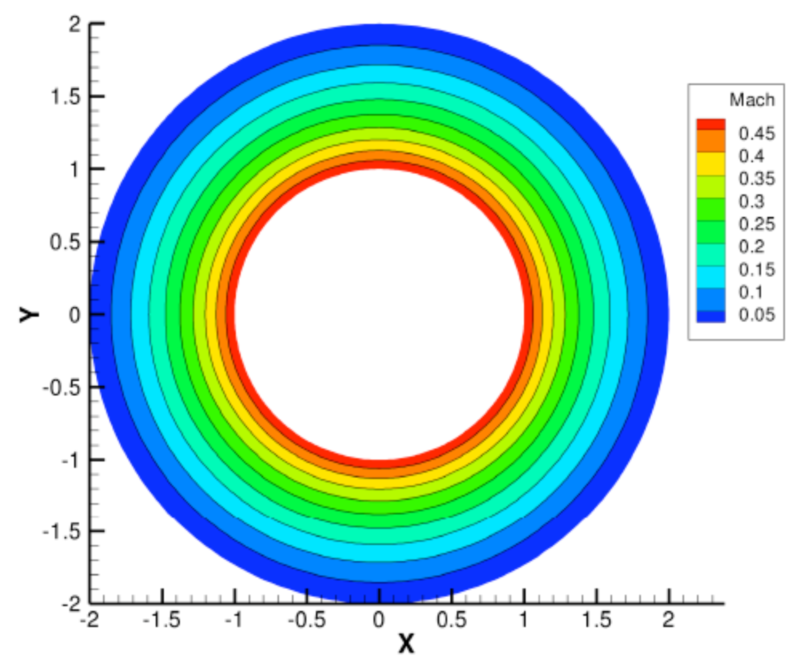

(b) Mach contour

Order Demonstration

No. of elements	No. of DOFs	L2-error	Order
3rd order SD			
48	432	8.896E-04	-
192	1728	1.002E-04	3.15
768	6912	1.084E-05	3.21
4th order SD			
48	768	1.4815E-04	-
192	3072	1.0036E-05	3.88
768	12288	6.5746E-07	3.93

- Exact solution of angular velocity $$v_\theta = \Omega_i r_i \frac{\frac{r_o}{r} - \frac{r}{r_o}}{\frac{r_o}{r_i} - \frac{r_i}{r_o}}$$

Oscillating Cylinder Computational Grid

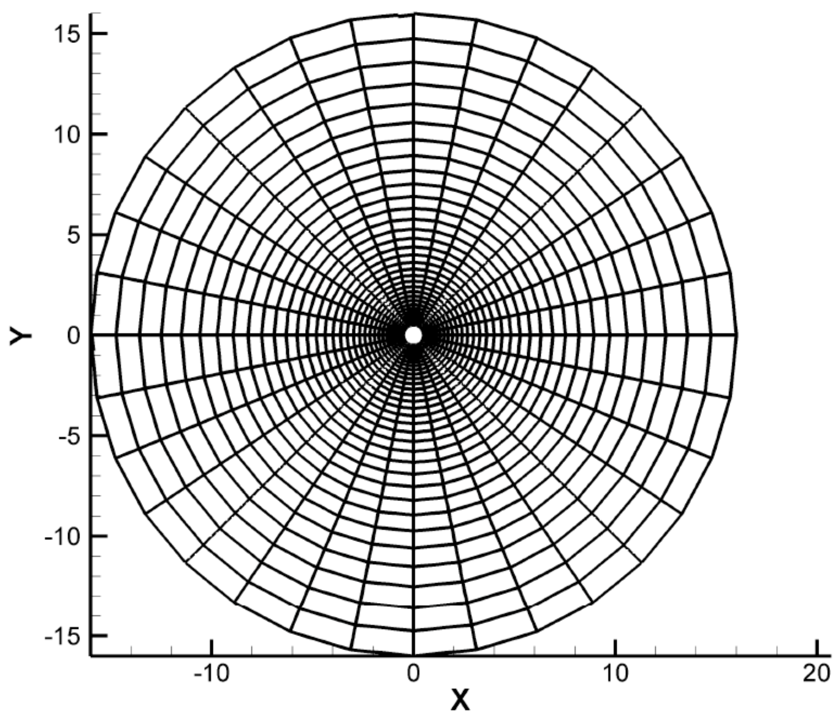

- Our simulation uses only 32x32 grid
- The third-order SD method
- Total degrees-of-freedom = 96x96
- Quadratic curved wall

Vorticity Behind An Oscillating Cylinder

- $y(t)=A_e*\cos(2*pi*f_e*t)$
- $A_e = 0.2D$
- $f_e = 1.1\ f_n$
- $-1<omega*d/U<1$
- Re =185

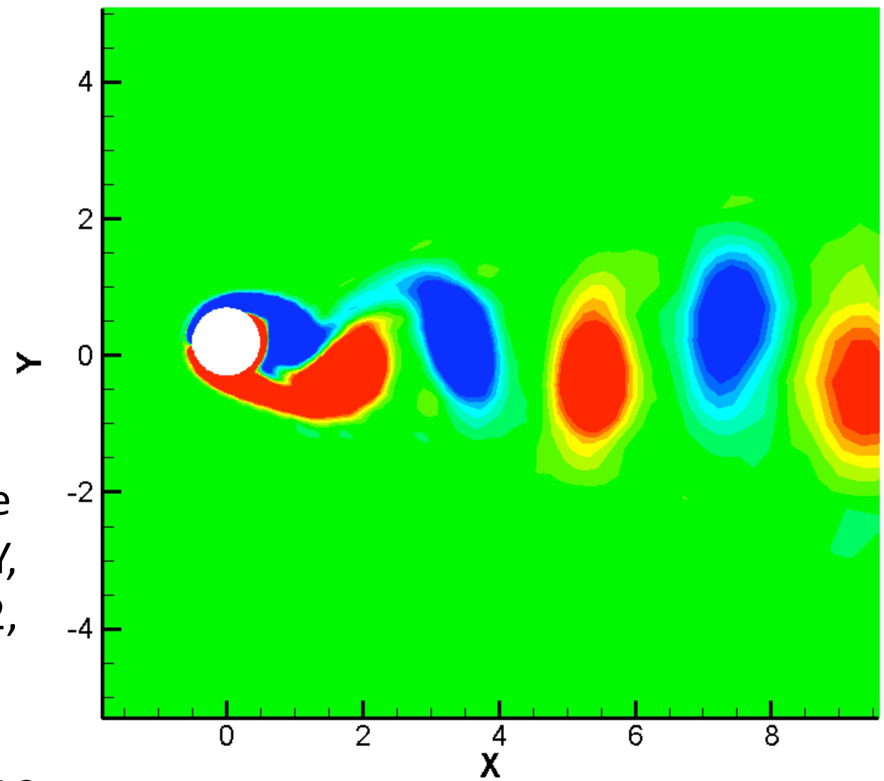

➢ The cylinder motion is identical to the one reported in E. GUILMINEAU and P. QUEUTEY, Journal of Fluids and Structures Vol 16, 2002, pp. 773-794

➢ We obtained nearly identical results using a grid with only 1024 cells compared to their 48,000 cell

Fluid-exerted Forces

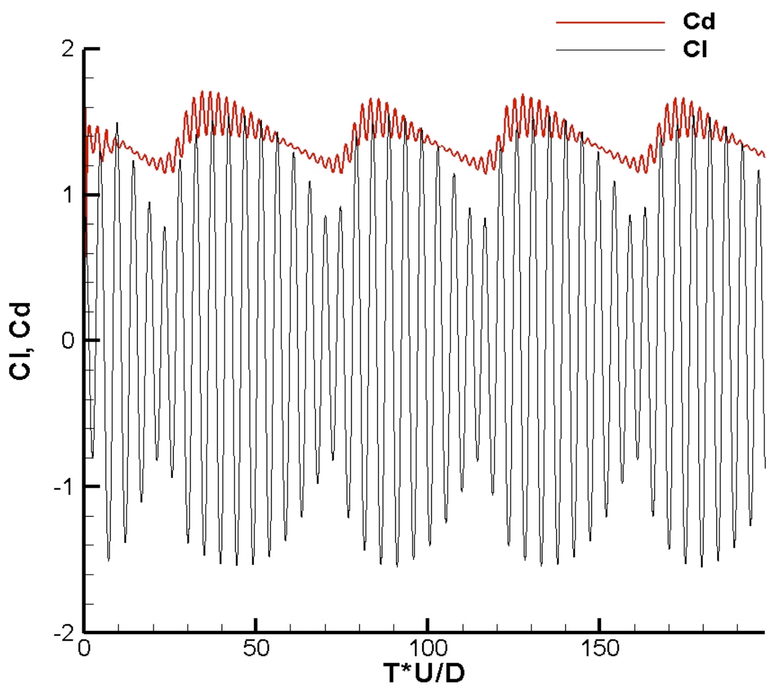

(a) Third order spectral difference

Total cell : 32x32

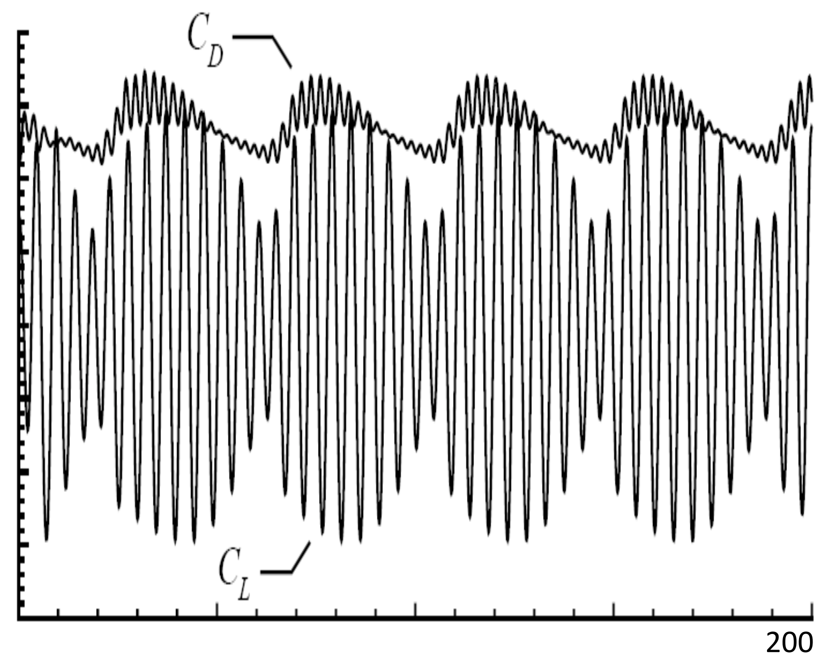

(b) E. GUILMINEAU and P. QUEUTEY
Journal of Fluids and Structures
Vol 16, 2002, pp. 773-794

Total cell : 240x200

The predicted force coefficients are in a good agreement with Guilmineau and Queutey (2002) and much less computational cells are used.

Numerical Results

Unsteady Flow Past Plunging Airfoil

NACA 0012 Grid with Mixed Elements

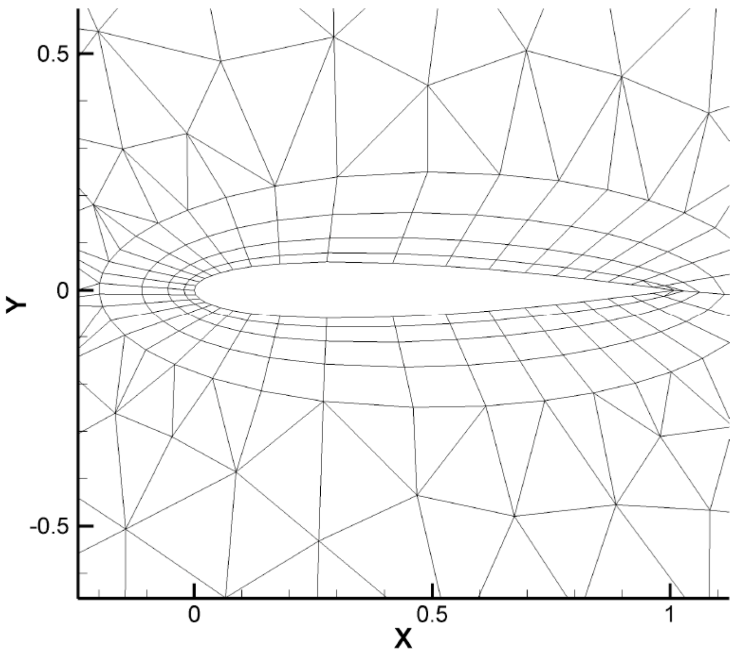

(a) Initial hybrid mesh: 'Mesh A'

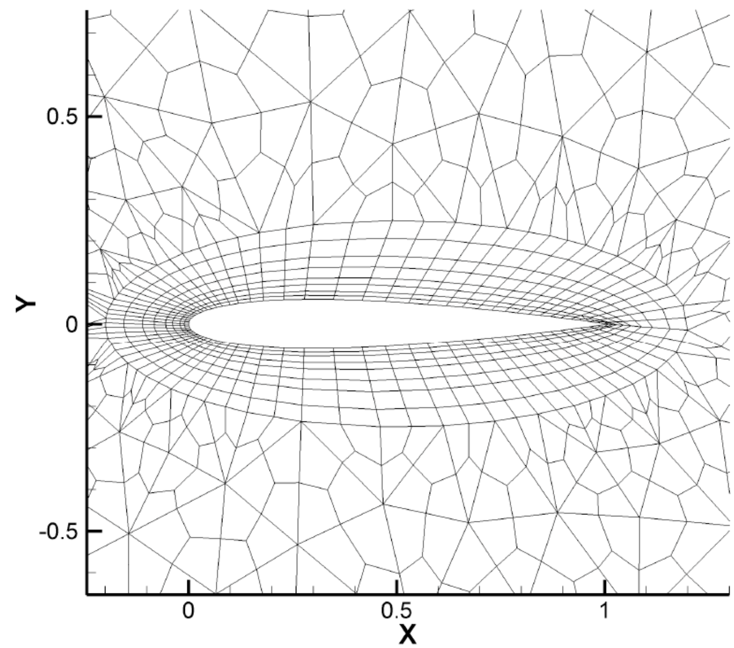

(b) One-level h-refinement: `Mesh B'

Viscous Flow Past a Stationary Airfoil

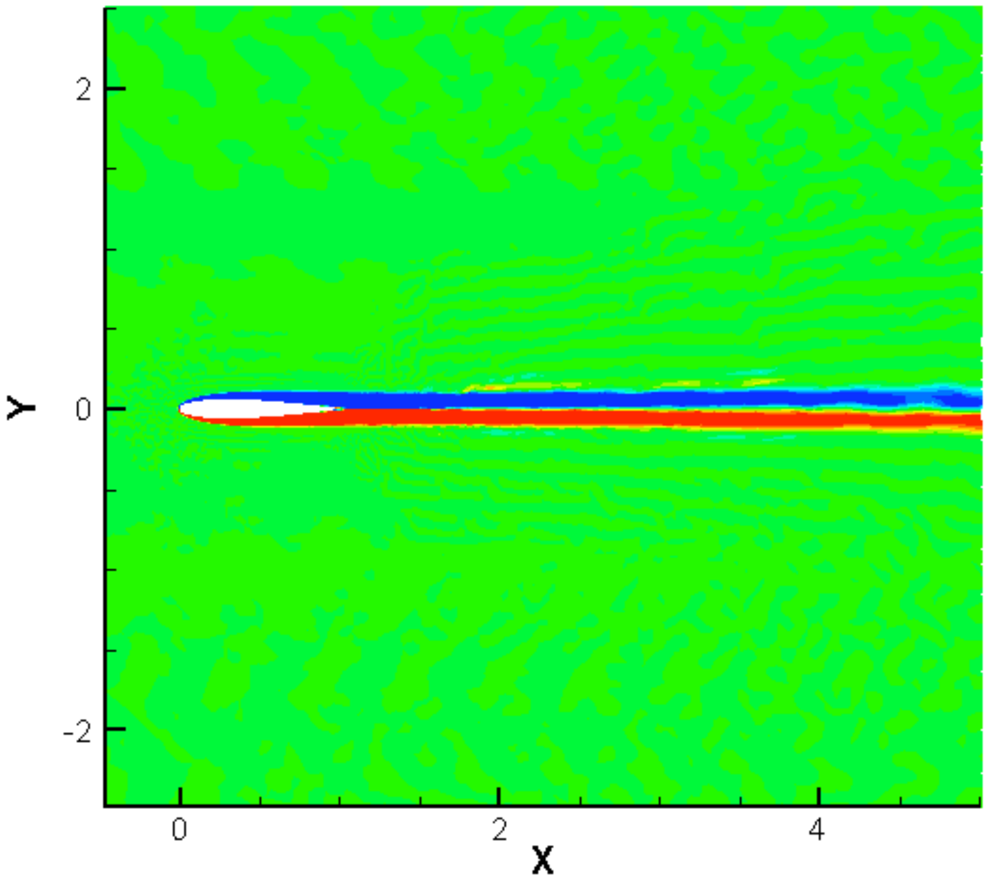

- Re = 1850
- Mach = 0.2
- Vortices: -5<Omega*c/U<5

Steady flow solution is reached eventually

Slow plunging airfoil case

- Y(t)=Ae*sin(omega*t)
- Omega = 1.15
- Ae = 0.08 c
- Chord c =1
- Mach = 0.2
- Uinf = 0.2
- Re=1850
- 4th order spectral difference method

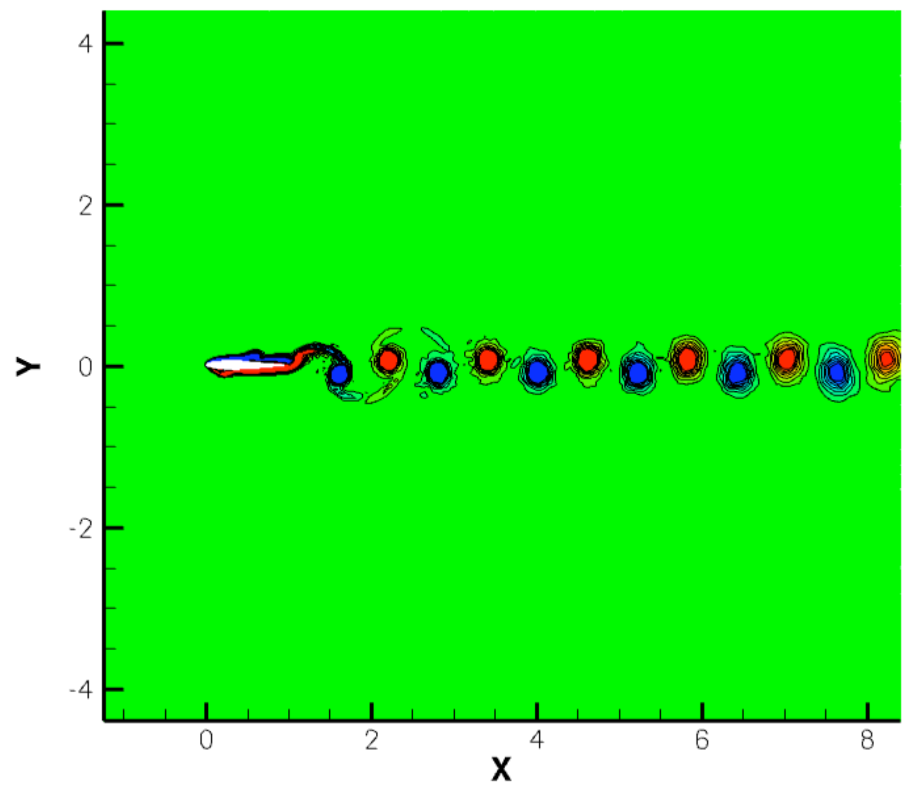

Force Coefficients for the Slowly Plunging Airfoil

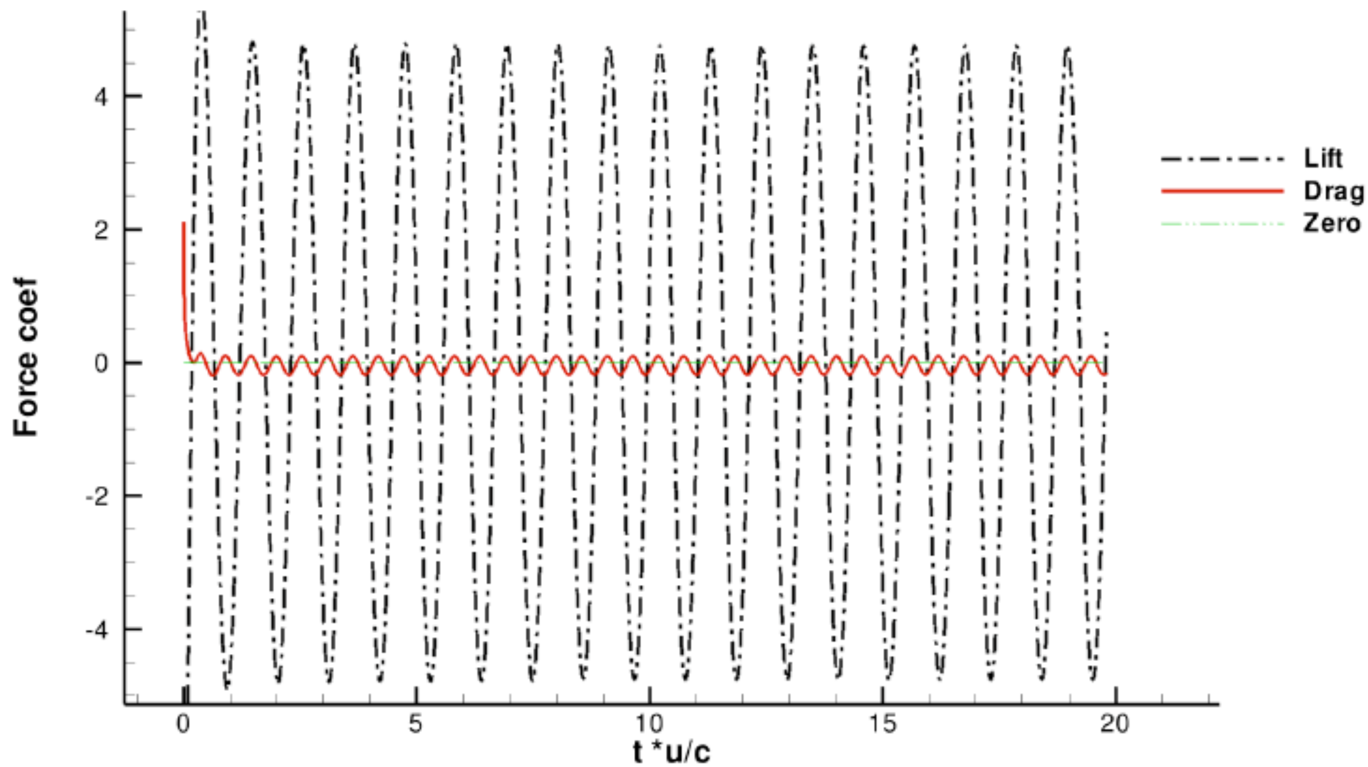

-4.78<Cl<4.77

-0.181<Cd<0.1

Mean drag coefficient = -0.0436

Fast Plunging Case

Our prediction suggested that the asymmetrical flow pattern depends on the direction of the airfoil's first stroke.

- First stroke of the airfoil goes upwards
- Y(t)=Ae*sin(omega*t)
- Omega = 2.46
- Ae = 0.12 c
- Chord c =1
- Mach = 0.2
- Uinf = 0.2
- Re=1850
- 3rd order spectral difference method

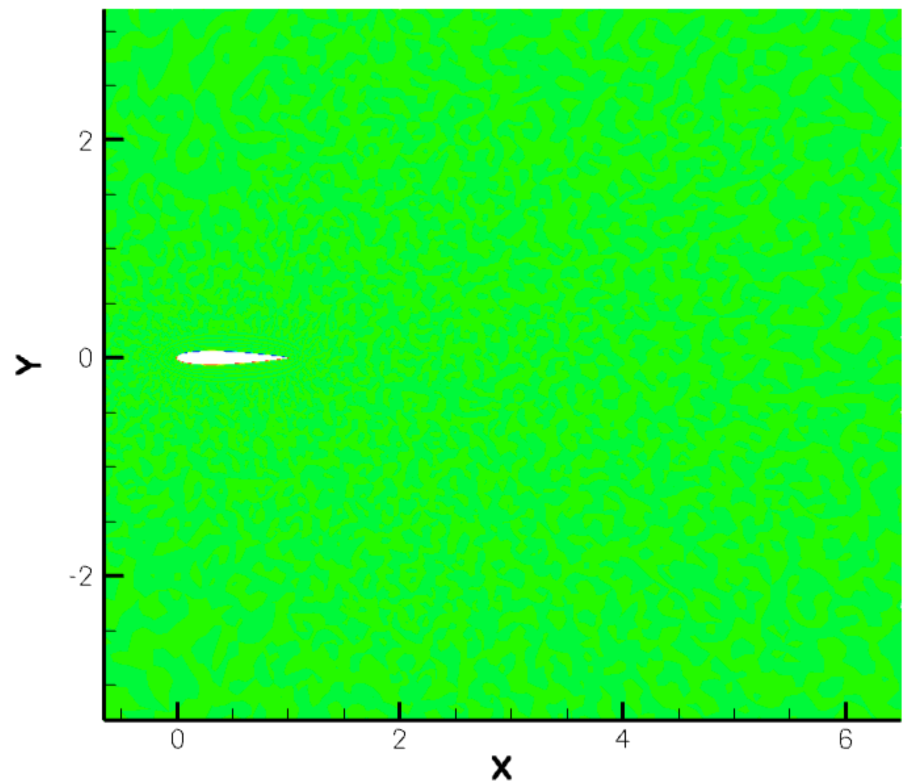

Fast Plunging, 3rd-order Simulation

- First stroke of the airfoil goes downwards
- Y(t)=Ae*sin(omega*t)
- Omega = 2.46
- Ae = 0.12 c
- Chord c =1
- Mach = 0.2
- U_inf =0.2
- Re=1850
- 3rd –order spectral difference method

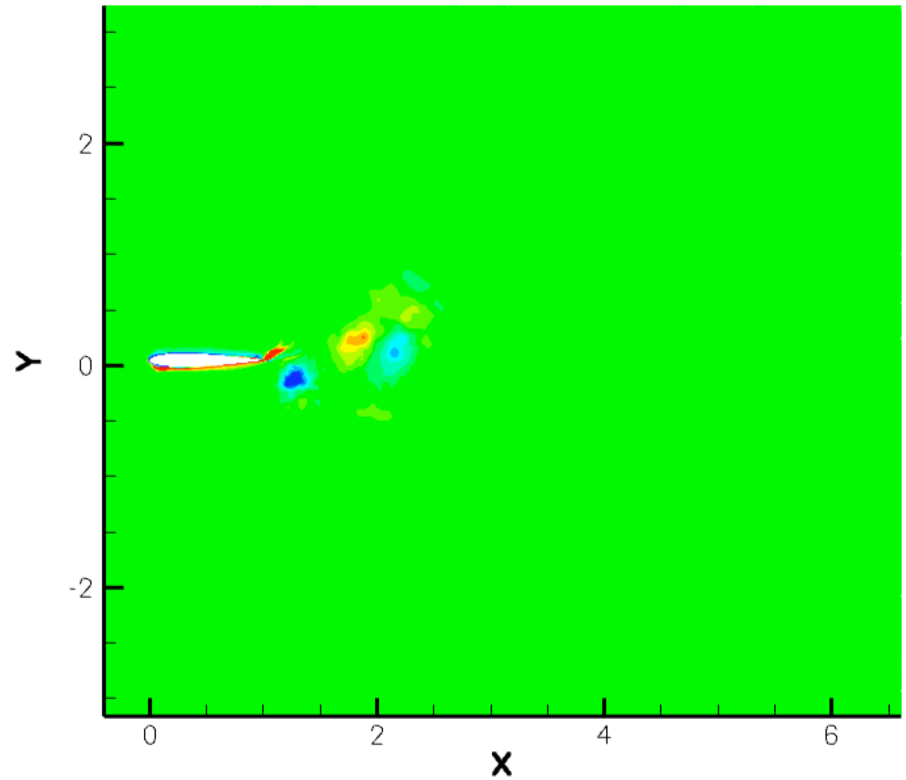

Simulation Comparison with Experiment

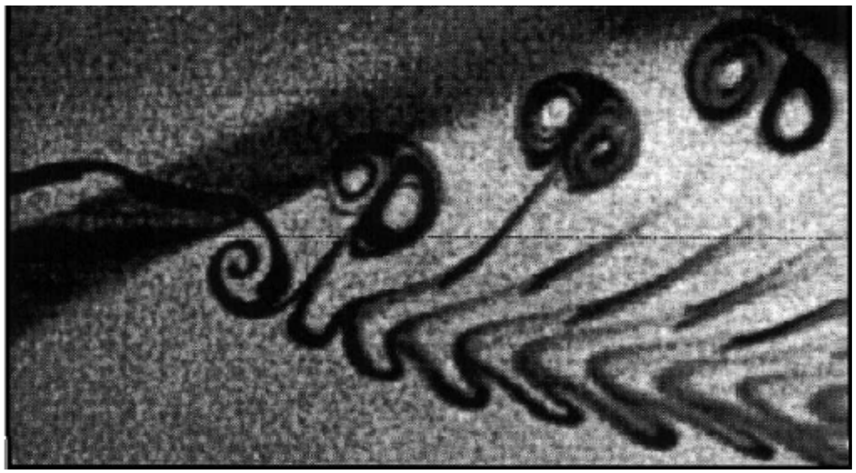

(a) Experiment by Jones, Dohring, and Platzer; AIAA JOURNAL Vol. 36, No. 7, July 1998

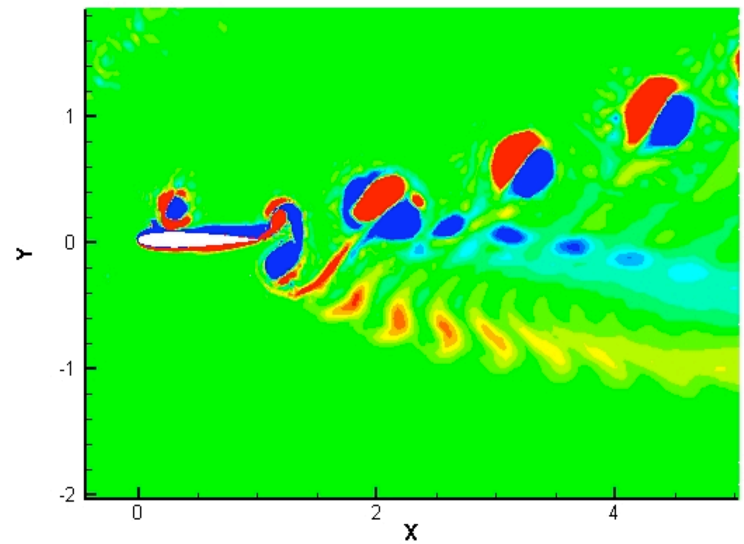

(b) 4th order Spectral difference method

Our prediction agrees better with the experimental results than any other published results !

- First stroke of the airfoil goes downwards
- Y(t)=Ae*sin(omega*t)
- Omega = 2.46
- Ae = 0.12 c

- Mach = 0.2
- Uinf = 0.2
- Re=1850
- Chord c=1

4^{th}-order SD Prediction for Plunging Airfoil

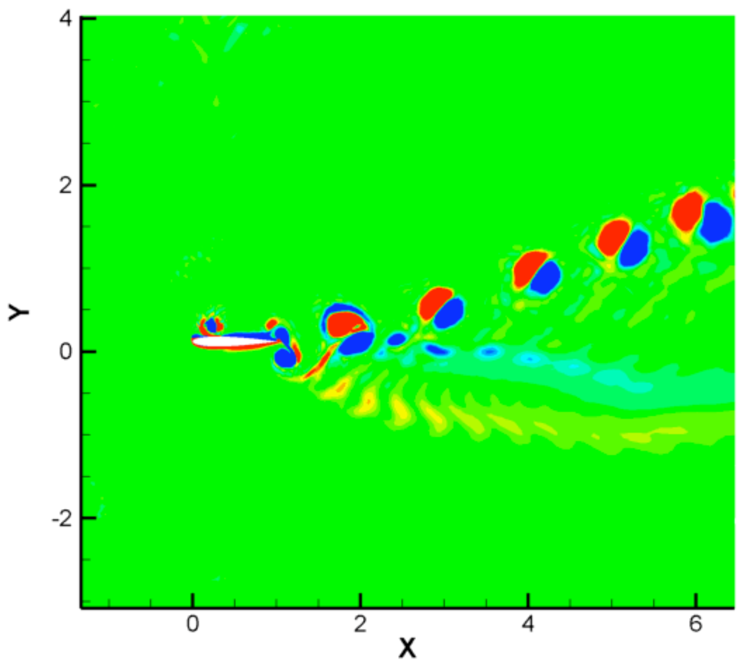

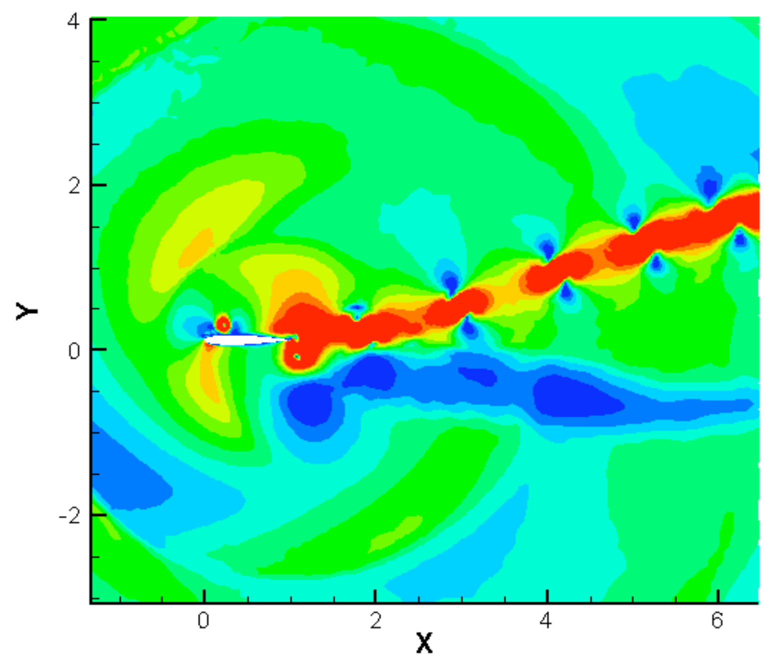

- Vorticity: -6<Omega*c/U<6
- Y(t)=Ae*sin(omega*t)
- Omega = 2.46
- Ae = 0.12 c

- Normalized velocity magnitude:
- 0.5<|V|/U_inf<2

Force Coefficients for Fast Plunging Case

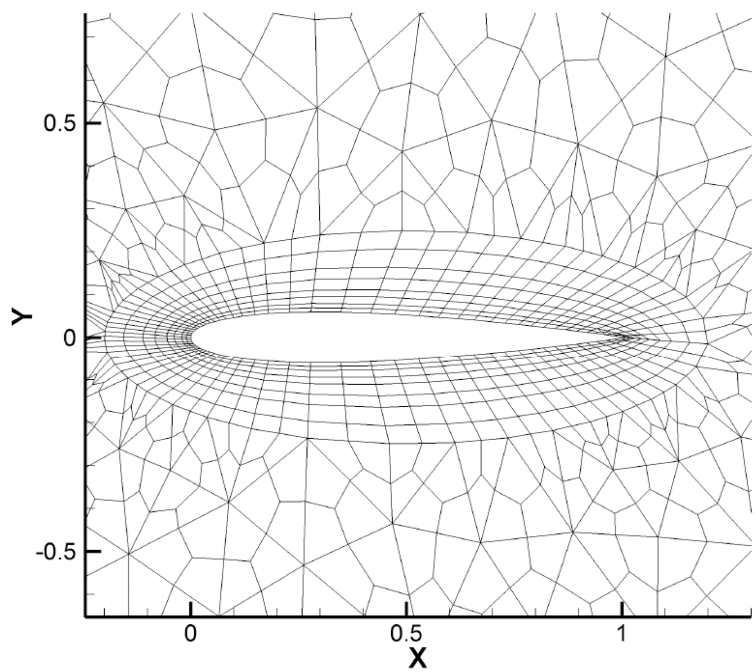

(a) Mesh B

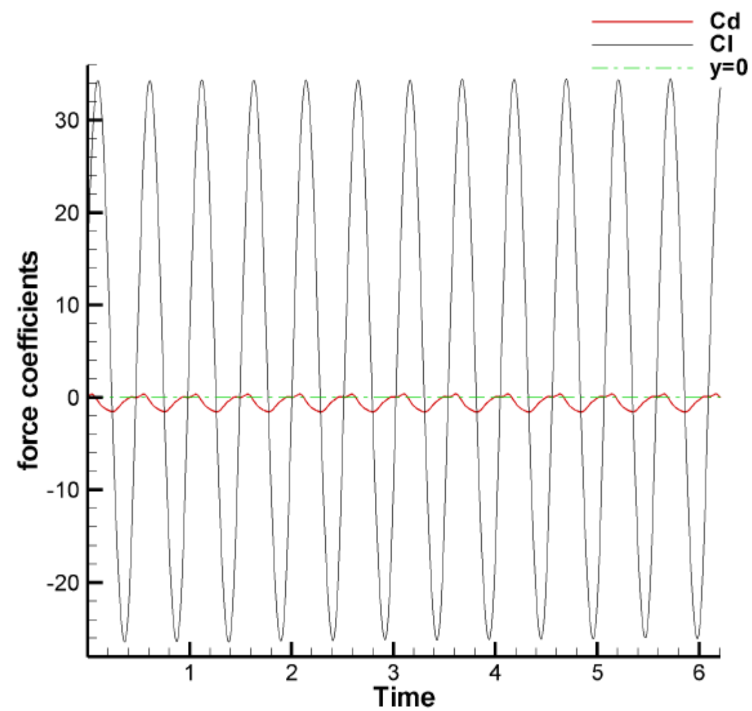

(b) the 4th order SD method;

-26 < Cl <34 Mean lift = 2.57

-1.51<Cd <0.37 Mean drag = -0.51

Flow on Moving Deforming Grids and Fluid Structure Interaction

Flow on Dynamic Deforming Mesh

Euler Vortex Propagation through Mesh with Deforming Mesh

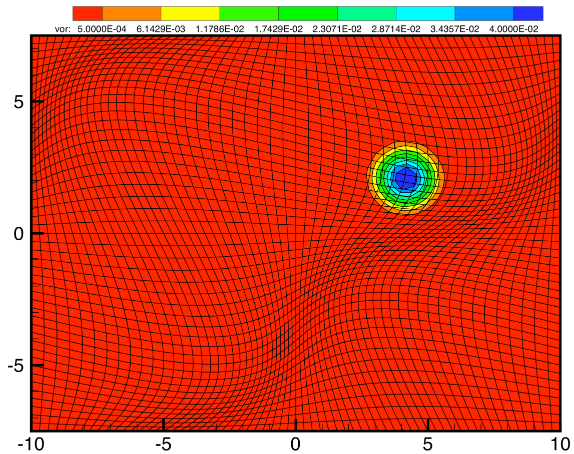

Vorticity in Physical Space

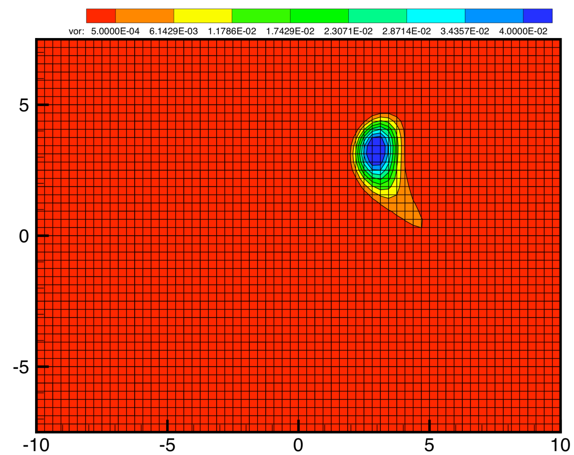

Vorticity in Reference Space

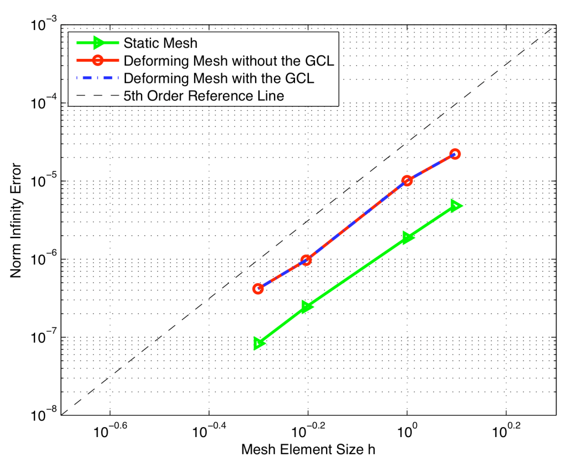

5th Order SD

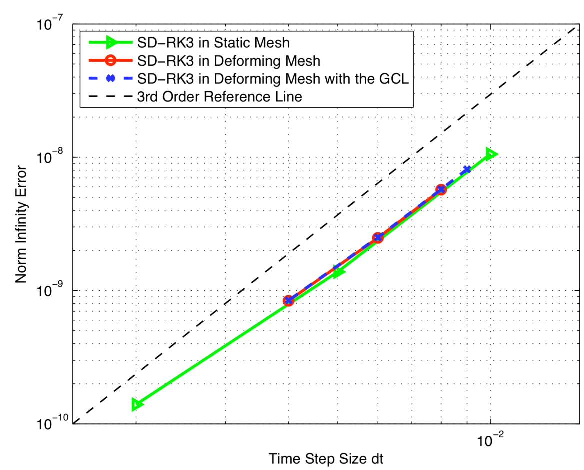

3rd Order RK

Euler Vortex Propagation Animations

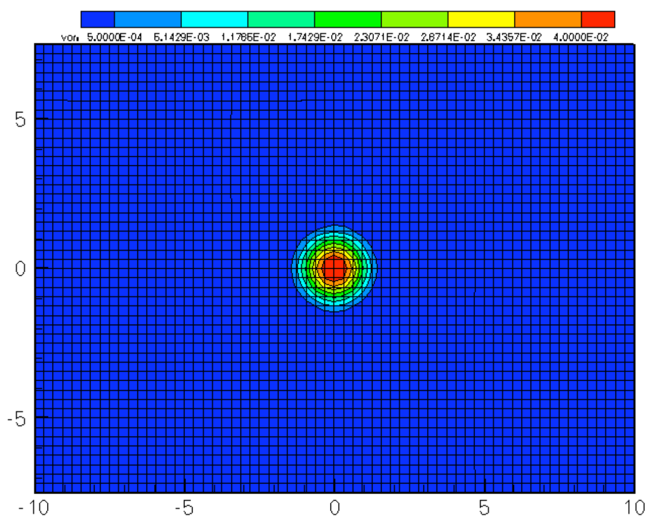

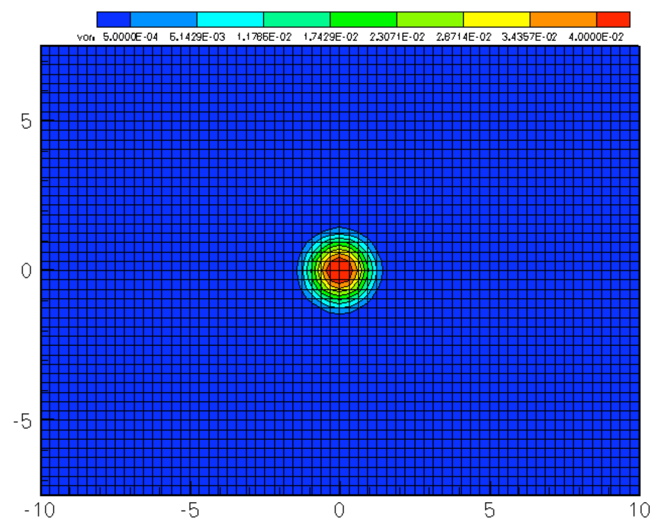

- Strength of the Euler Vortex = 0.3
- Velocity in x = 0.4472; Velocity in y = 0.2236
- 5th Order SD Method

Mesh Deformation Method

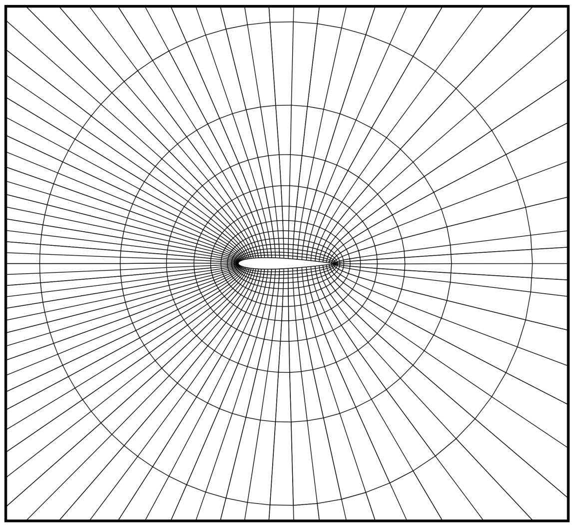

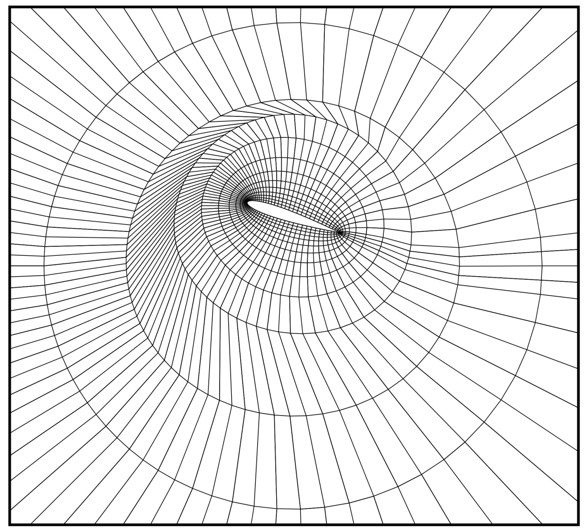

- Rigid Mesh Displacement Near Field around the Boundary
- Fixed Mesh at Far Field Boundary
- Smooth Mesh Deformation/Blending with High Order Polynomial

Mesh Deformation Animations

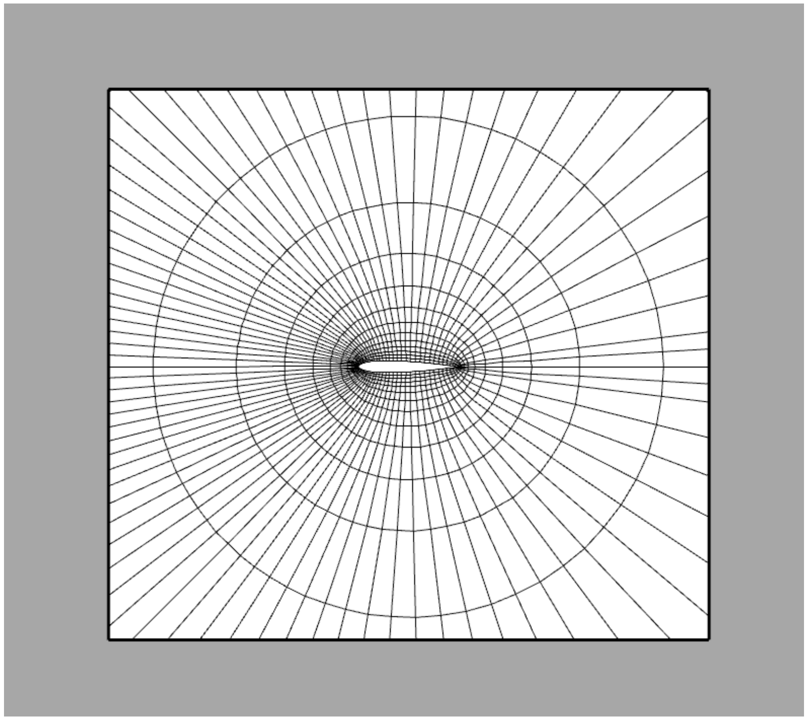

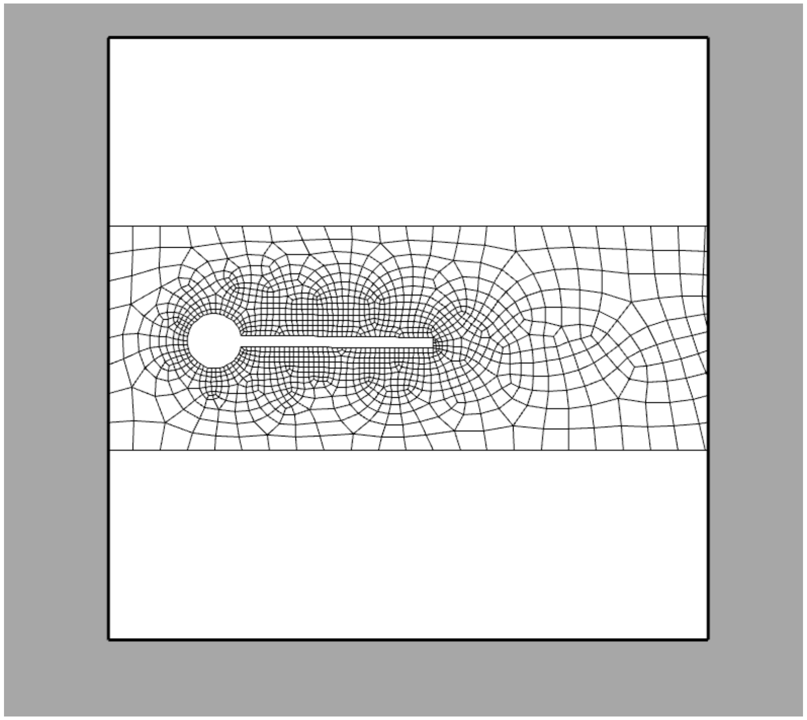

Plunging Airfoil on Dynamic Deforming Mesh

Comparison of Computation and Experiment Results for Flow over a Plunging Airfoil

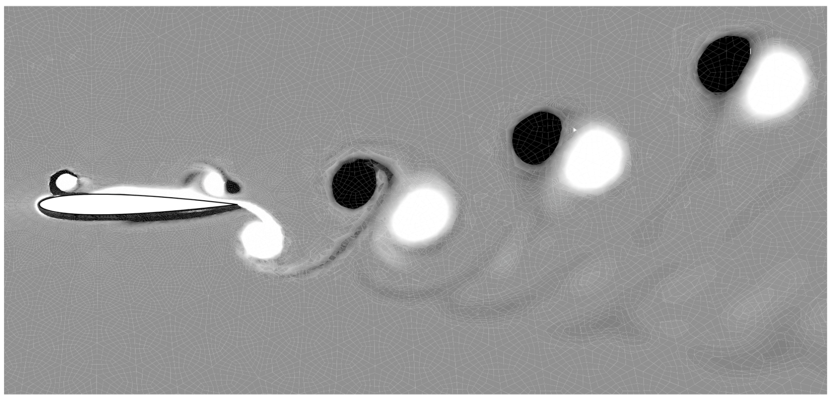

Computation Result

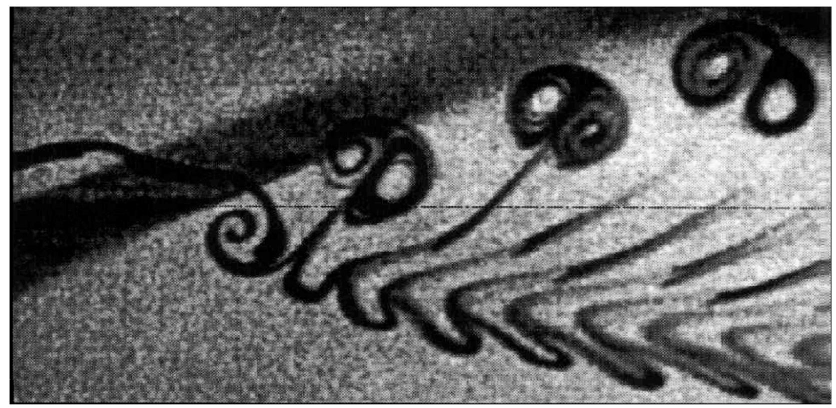

Experiment Result

- Near Identical Result Compared with the Rigid Mesh Case

Extension to Fluid Structure Interaction

Low Mach Number Flow over a Cylinder Beam Configuration

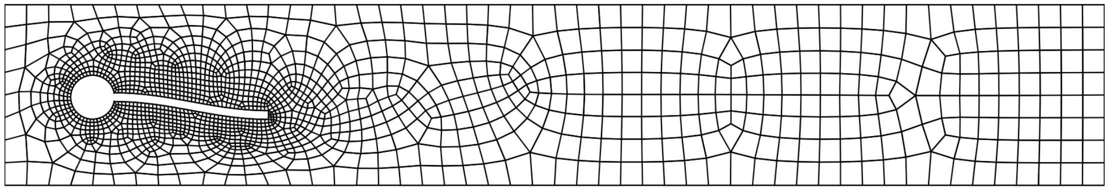

Mesh

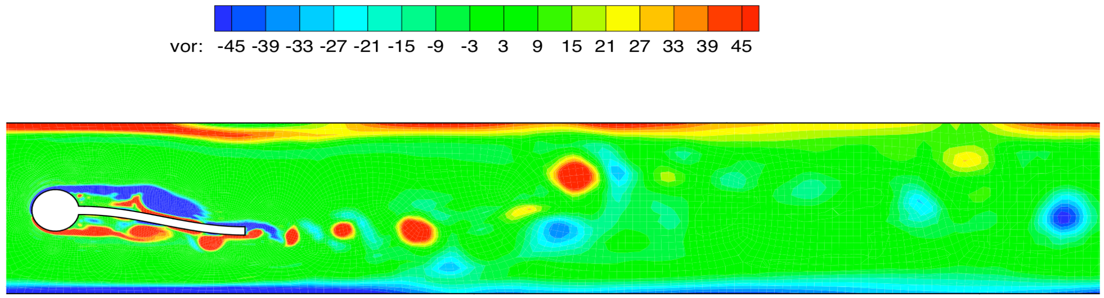

Vorticity

- Beam deforms with Prescribed Sinusoidal Motion
- U=0.1; Mach=0.01 ; Re=100
- Fluid Structure Coupling is Work in Progress

Fluid Structure Interaction Animation

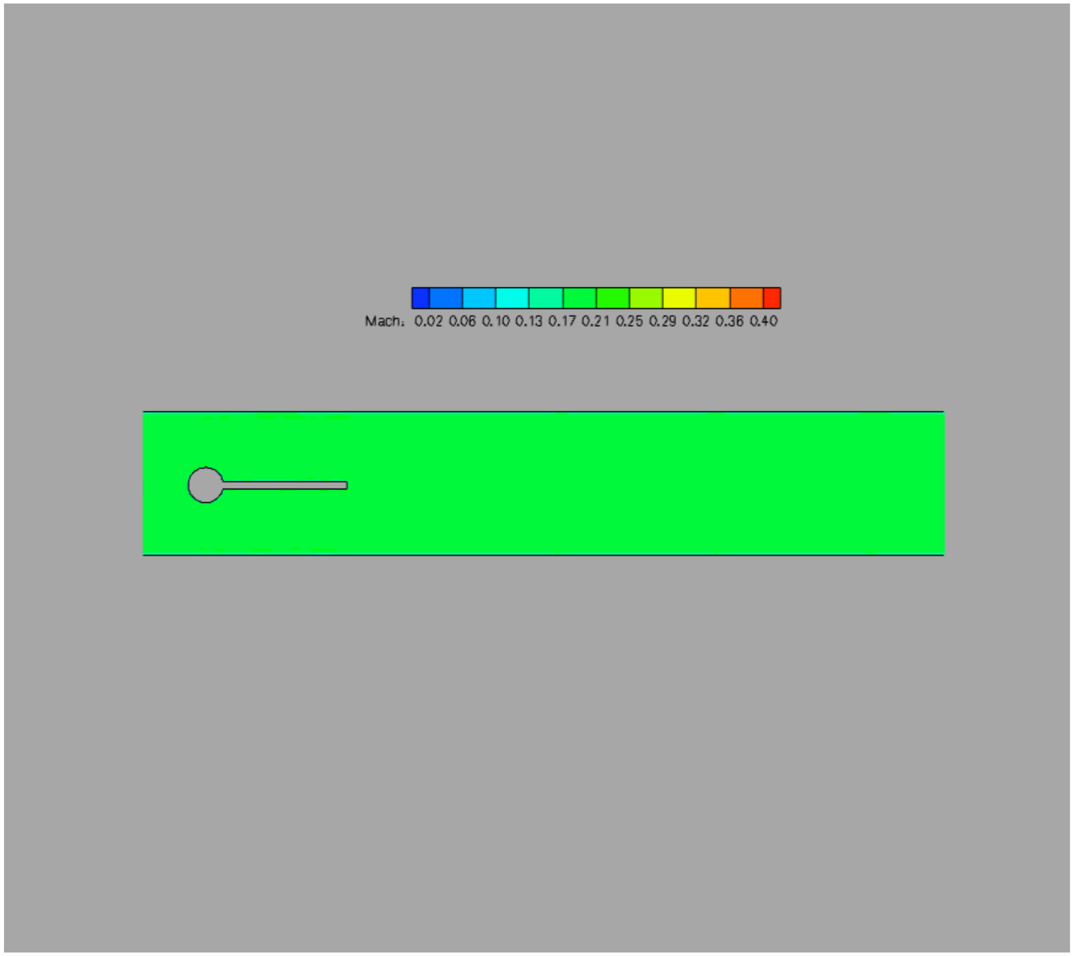

Adaptive Mesh Refinement

Adaptive Mesh Refinement

Test Case: NACA0012 Airfoil, M=0.5, Steady Inviscid Flow

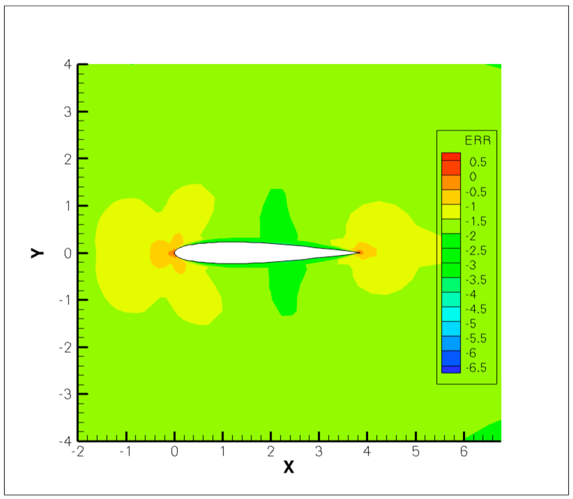

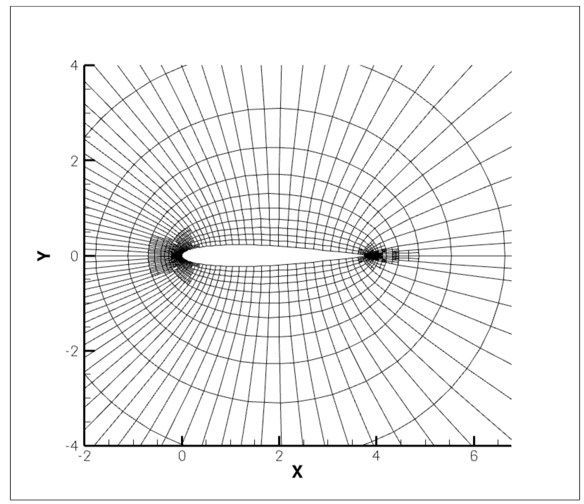

- Error Indicator 1:

  Unweighted Residual $|R(Q^H_h)|$

- Adapted Mesh Showing Refined Mesh at the Leading and Trailing Edge

Adaptive Mesh Refinement

Test Case: NACA0012 Airfoil, M=0.5, Steady Inviscid Flow

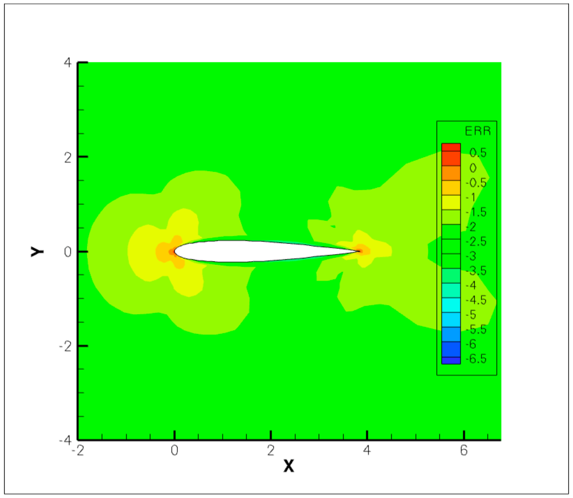

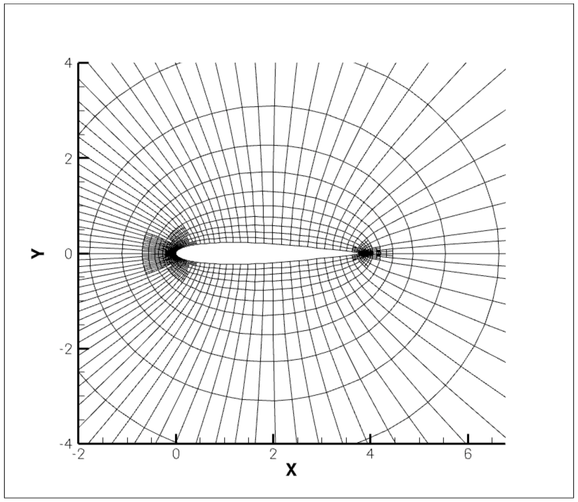

- Error Indicator 2:

  Entropy Adjoint $|(V^H_h)^T R(Q^H_h)|$

- Adapted Mesh Showing Refined Mesh at the Leading and Trailing Edge

Shock Capturing using Artificial Viscosity

Shock Capturing using Artificial Viscosity

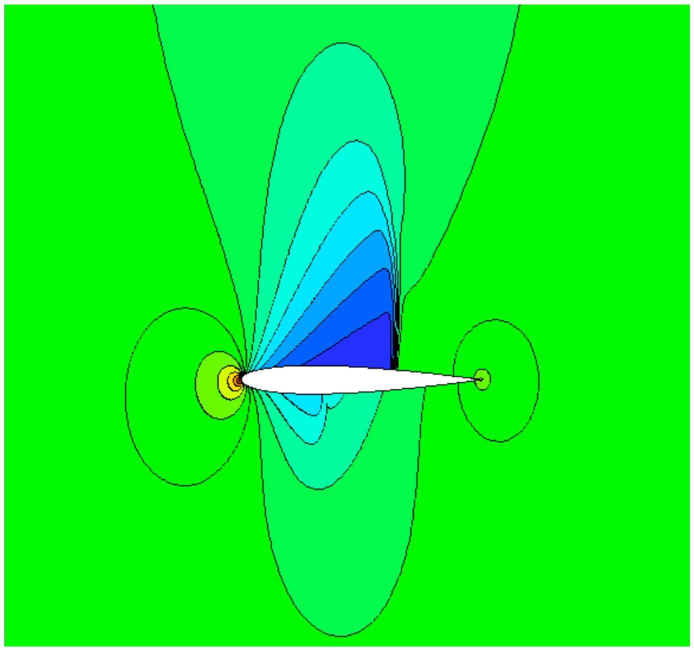

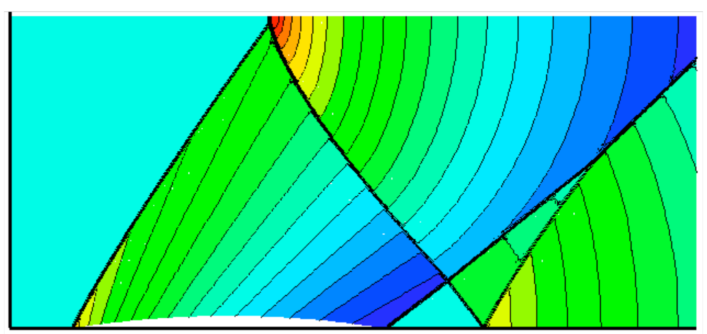

- Use of artificial bulk viscosity with a dilatation sensor
- Artificial viscosity is switched on only in regions of strong negative dilatation (shocks)
- Smooth variation of artificial viscosity

Shock Capturing using Artificial Viscosity

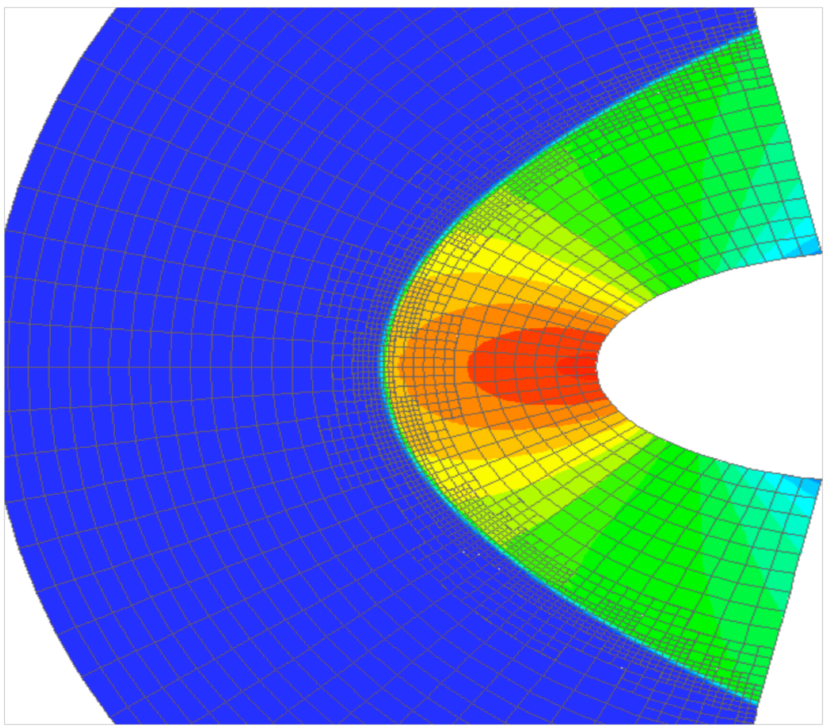

- Use of adaptive mesh refinement in combination with artificial viscosity

Turbulence Transition for 3D Wing

Turbulent Transition for 3D Wing

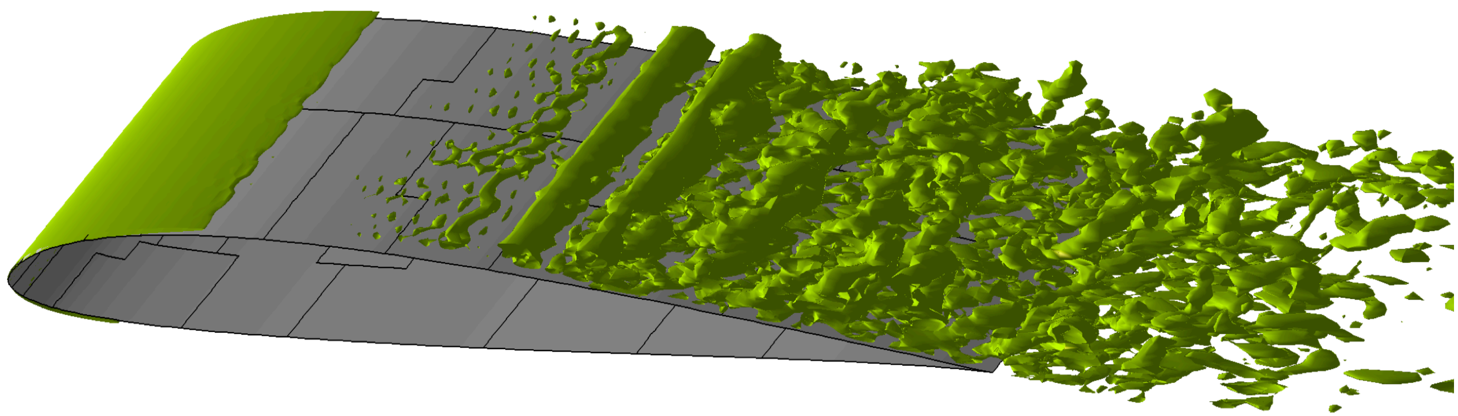

- Test case: Transitional Flow over SD7003 airfoil at 4 degrees AOA and Re=60000
- Code: 3D, parallel, unstructured solver for Navier-Stokes equations, NO sub-grid models

Turbulent Transition for 3D Wing

Results: Good agreement with computational and experimental results

Data Set	Freestream Turbulence	Separation x_{sep}	Transition x_{tr}/c	Reattachment x_r/c
TU-BS (Experiment)	0.08%	0.30	0.53	0.64
HFWT (Experiment)	0.1%	0.18	0.47	0.58
Visbal (ILES)	0	0.23	0.55	0.65
Uranga (ILES, DG)	0	0.23	0.51	0.60
Present ILES	0	0.23	0.53	0.64

Spectral Difference Stability Proof

Nodal DG Method Stability Proof

Local Vectors

$$\mathbf{u}^T = [u_1, \ldots u_n]$$

$$\mathbf{f} = a\mathbf{u}$$

$$\mathbf{l}^T = [l_1, \ldots l_n]$$

Mass and Stiffness Matrices

$$\mathbf{M}_{ij} = \int_1^{-1} l_i l_j dx$$

$$\mathbf{S}_{ij} = \int_1^{-1} l_i l_j' dx$$

Matrix Representation of the Weak Form

$$\mathbf{M}\frac{d\mathbf{u}}{dt} - \mathbf{S}^T\mathbf{f} + \hat{f}\mathbf{l}\Big|_1^{-1} = 0$$

Matrix Representation of the Strong Form

$$\mathbf{M}\frac{d\mathbf{u}}{dt} + \mathbf{S}\mathbf{f} + (\hat{f} - f)\mathbf{l}\Big|_1^{-1} = 0$$

Nodal DG Method Stability Proof

Multiplying the linear advection equation by u and integrating over x,

$$\int_a^b u\frac{\partial u}{\partial t}dx = -a\int_a^b u\frac{\partial u}{\partial x}dx = -a\int_a^b \frac{\partial(\frac{u^2}{2})}{\partial x}dx$$

Thus it satisfies the energy estimate

$$\frac{d}{dt}\int_a^b \frac{u^2}{2}dx = \frac{1}{2}a(u_a^2 - u_b^2)$$

Nodal DG Method Stability Proof

Multiply the strong form by the local solution $\mathbf{u}^{\mathbf{T}}$ to obtain,

$$\mathbf{u}^T \mathbf{M} \frac{d\mathbf{u}}{dt} + \mathbf{u}^T \mathbf{S} \mathbf{f} + \mathbf{u}^T \mathbf{I} (\hat{f} - f) \Big|_{x_L}^{x_R} = 0$$

Since **M** and **S** are pre-integrated exactly, this is equivalent to

$$\frac{d}{dt} \int_{x_L}^{x_R} \frac{u_h^2}{2} dx + a \int_{x_L}^{x_R} u_h \frac{\partial u_h}{\partial x} dx + u_h (\hat{f} - a u_h) \Big|_{x_L}^{x_R} = 0$$

Then integrate the middle term and combine it with the last term,

$$\frac{d}{dt} \int_{x_L}^{x_R} \frac{u_h^2}{2} dx = -(u_h \hat{f} - a \frac{u_h^2}{2}) \Big|_{x_L}^{x_R}$$

Nodal DG Method Stability Proof

In the interior interface collecting the contributions elements on the left and right sides, there is a total negative contribution of

$$
\begin{aligned}
& u_R\hat{f} - a\frac{u_R^2}{2} - (u_L\hat{f} - a\frac{u_L^2}{2}) \\
=& \frac{1}{2}a(u_R^2 - u_L^2) - \frac{1}{2}\alpha|a|(u_R - u_L)^2 - \frac{1}{2}a(u_R^2 - u_L^2) \\
=& -\frac{1}{2}\alpha|a|(u_R - u_L)^2 \implies \textit{negative contribution at every interior interface}
\end{aligned}
$$

At the two end boundaries,

- Extrapolated upwind flux $f_b = au_h$ at outflow boundary $\implies$ negative contribution
- Use the true flux $f_a = au_a$ at inflow boundary $\implies$ positive but less than the true inflow boundary contribution $au_au_h - \frac{1}{2}au_h^2 = \frac{1}{2}au_a^2 - \frac{1}{2}a(u_a - u_h)^2 < \frac{1}{2}au_a^2$

Energy Stability of DG

This completes the proof that the DG scheme is energy stable for the linear advection equation.

Spectral Difference Method Stability Proof

Interior Flux and Boundary Flux Correction

$$f = au$$

$$\hat{f}(-1) = au_h(-1) + f_{CL},\ \hat{f}(1) = au_h(1) + f_{CR}$$

$$f_{CL} = \hat{f}(-1) - au_h(-1),\ f_{CR} = \hat{f}(1) - au_h(1)$$

Upon substitution, and noting $u_h(x)$ is a polynomial of degree p hence exactly represented by the sum, the flux becomes,

Flux Reconstruction (Follow the Procedure Proposed by Huynh)

$$f_h(x) = \sum_{j=1}^{n+1} f_j \hat{l}_j(x) \implies f_h(x) = f_{CL}\hat{l}_1(x) + f_{CR}\hat{l}_{n+1}(x) + a\sum_{j=1}^{n+1} u_h(\hat{x}_j)\hat{l}_j(x)$$

$$\implies f_h(x) = f_{CL}\hat{l}_1(x) + f_{CR}\hat{l}_{n+1}(x) + au_h(x)$$

Spectral Difference Method Stability Proof

Rewrite the SD scheme as

$$\frac{\partial u_h}{\partial t} = -\frac{\partial f_h}{\partial x} \implies \frac{\partial u_h}{\partial t} = -a\frac{\partial u_h}{\partial x} - f_{CL}\hat{l}_1' - f_{CR}\hat{l}_{n+1}'$$

Evaluating this at the solution points

$$\begin{aligned}\frac{du_i}{dt} &= -\, a\sum_{j=1}^{n} \mathbf{D}_{ij}u_j - f_{CL}\hat{l}_1'(x_i) - f_{CR}\hat{l}_{n+1}'(x_i) \\ &\implies -\, a\sum_{j=1}^{n} \mathbf{D}_{ij}u_j - f_{CL}\hat{l}_1'(x_i) \textit{ for upwind numerical flux}\end{aligned}$$

where $\mathbf{D} = \mathbf{M}^{-1}\mathbf{S}$ is the differentiation matrix associated with the solution collocation points, and is uniquely determined by the points location and the polynomial degree p.

Spectral Difference Method Stability Proof

The SD scheme can be converted to a form which resembles the nodal DG method by multiplying it by the mass matrix to produce

SD Scheme in NDG Form

$$\sum_j \mathbf{M}_{ij} \frac{du_j}{dt} + a \sum_j \mathbf{S}_{ij} u_j = -f_{CL} \sum_j \mathbf{M}_{ij} \hat{l}_1'(x_j)$$

Now since $\hat{l}_1(-1) = 1$ and $\hat{l}_1(1) = 0$,

Boundary Flux

$$\begin{aligned}\sum_{j=1}^{n} \mathbf{M}_{ij} \hat{l}_1'(x_j) &= \int_{-1}^{1} l_i(x) \sum_{j=1}^{n} \hat{l}_1'(x_j) l_j(x) dx = \int_{-1}^{1} l_i(x) \hat{l}_1'(x) dx \\ &= \hat{l}_1 l_i \Big|_{-1}^{1} - \int_{-1}^{1} l_i'(x) \hat{l}_1(x) dx = -l_i(-1) - \int_{-1}^{1} l_i'(x) \hat{l}_1(x) dx\end{aligned}$$

Spectral Difference Method Stability Proof

Upon substitution the resulting SD scheme becomes,

SD Scheme

$$\sum_j \mathbf{M}_{ij} \frac{du_j}{dt} + a \sum_j \mathbf{S}_{ij} u_j = f_{CL} \left(l_i(-1) + \int_{-1}^{1} l_i'(x) \hat{l}_1(x) dx \right)$$

which differs from the corresponding nodal DG equation,

NDG Scheme

$$\sum_j \mathbf{M}_{ij} \frac{du_j}{dt} + a \sum_j \mathbf{S}_{ij} u_j = f_{CL} \Big(l_i(-1) \Big)$$

only in the last term.

Spectral Difference Method Stability Proof

In order to make the last term in the SD scheme equal to the nodal DG scheme, we consider the following strategy by replacing the mass matrix $\mathbf{M}$ by a matrix $\mathbf{Q} > 0$ such that it will eventually cause a cancellation of the desired terms.

Choice of New Mass Matrix

$$\mathbf{Q} = \mathbf{M} + \mathbf{C}$$

$$\mathbf{QD} = (\mathbf{M} + \mathbf{C})\mathbf{D} = \mathbf{MD} + \mathbf{CD} = \mathbf{S} \implies \mathbf{CD} = 0$$

Thus each row of $\mathbf{C}$ must be orthogonal to every column of $\mathbf{D}$.

Spectral Difference Method Stability Proof

In order to find a row vector which is orthogonal to every column of **D**, consider

p^{th} difference operator d^T

$$\sum_{j=1}^{n} d_j R_p(x_j) = R_p^{(p)}$$

for any polynomial of degree p.

Then further operation by the differentiation matrix **D** gives

$$\sum_i d_i \sum_j D_{ij} R_p(x_j) = R_p^{(p+1)} = 0$$

Thus we find the desired matrix **C** that is orthogonal to **D**

$$Q = M + C = M + cdd^T, \ with \ C = cdd^T$$

where c is an arbitrary parameter.

Spectral Difference Method Stability Proof

SD Scheme using Mass Matrix Q

$$\sum_j \mathbf{Q}_{ij} \frac{du_j}{dt} + a \sum_j \mathbf{S}_{ij} u_j = -f_{CL} \sum_j \mathbf{M}_{ij} \hat{l}_1'(x_j) - f_{CL} \sum_j \mathbf{C}_{ij} \hat{l}_1'(x_j)$$

Extra Term

$$-f_{CL} \sum_j \mathbf{C}_{ij} \hat{l}_1'(x_j) = -c\, f_{CL}\, d_i \sum_j d_j \hat{l}_1'(x_j) = -c\, f_{CL}\, \hat{l}_1^{(p+1)} l_i^{(p)}$$

SD Scheme using Mass Matrix Q

$$\sum_j \mathbf{Q}_{ij} \frac{du_j}{dt} + a \sum_j \mathbf{S}_{ij} u_j = f_{CL} \left(l_i(-1) + \int_{-1}^{1} l_i'(x) \hat{l}_1(x) dx - c\, \hat{l}_1^{(p+1)} l_i^{(p)} \right)$$

Spectral Difference Method Stability Proof

Now if we can choose c so that the last two terms on the right cancel, we can attain an energy estimate with the norm $\mathbf{u}^T\mathbf{Q}\mathbf{u}$ replacing $\mathbf{u}^T\mathbf{M}\mathbf{u}$ in each element.

Required Cancellation

$$f_{CL}\int_{-1}^{1} l_i'(x)\hat{l}_1(x)dx = f_{CL}c\,\hat{l}_1^{(p+1)}l_i^{(p)}$$

Spectral Difference Method Stability Proof

Thus the desired cancellation is obtained by setting

Cancellation Constant

$$c = \frac{2p}{2p+1}\frac{1}{c_p^2}\frac{1}{p!(p+1)!} > 0$$

In the case that the interface flux is not fully upwind, a similar calculation shows that the convection from the right boundary is correspondingly reduced, so that finally

SD Scheme Cast in Nodal DG Form

$$\sum_j \mathbf{Q}_{ij}\frac{du_j}{dt} + a\sum_j \mathbf{S}_{ij}u_j = f_{CL}l_i(-1) - f_{CR}l_i(1)$$

Spectral Difference Method Stability Proof

Since u_h is a polynomial of degree p, $\sum_i d_i u_i = u_h^{(p)}$, and in each element, allowing for the scaling factor $\beta = \frac{x_R - x_L}{2}$ in the transformation from the reference element

$$\sum_i \sum_j u_i \mathbf{Q}_{ij} u_j = \frac{1}{\beta} \int_{xL}^{xR} (u_h^2 + \beta^{2p}\, c\, u_h^{(p)^2}) dx$$

Now the same argument that was used to prove the energy stability of the nodal DG scheme establishes the energy stability of the SD scheme with the norm

$$\int_a^b (u_h^2 + \beta^{2p}\, c\, u_h^{(p)^2}) dx$$

with the piecewise constant scaling factor β, for the case of solution polynomials of degree p, provided that the interior flux collocation points are the zeros of $L_p(x)$.

Concluding Remarks

Conclusions

✓Unstructured grid spectral difference method 2D/3D solvers have been successfully developed in our group

✓The SD method 2D solver is able to model compressible viscous flow with moving boundaries with high accuracy

✓Promising Results obtained for 3D Wing Transition Prediction, Shock Capturing, Moving Deforming Mesh, and Adaptive Mesh Refinement

✓The SD method for the 1D linear advection equation is stable for all orders of accuracy in an energy norm of Sobolev type.